


Article

Oxygen Depletion and the Role of Cellular Antioxidants in FLASH Radiotherapy: Mechanistic Insights from Monte Carlo Radiation-Chemical Modeling

Israth Rabeya, Jintana Meesungnoen and Jean-Paul Jay-Gerin * 

Department of Medical Imaging and Radiation Sciences, Faculty of Medicine and Health Sciences, Université de Sherbrooke, 3001, 12th Avenue Nord, Sherbrooke, QC J1H 5N4, Canada; israth.rabeya@usherbrooke.ca (I.R.); jintana.meesungnoen@usherbrooke.ca (J.M.)

* Correspondence: jean-paul.jay-gerin@usherbrooke.ca

Abstract: FLASH radiotherapy is a novel irradiation modality that employs ultra-high mean dose rates exceeding 40–150 Gy/s, far surpassing the typical ~0.03 Gy/s used in conventional radiotherapy. This advanced technology delivers high doses of radiation within milliseconds, effectively targeting tumors while minimizing damage to the surrounding healthy tissues. However, the precise mechanism that differentiates responses between tumor and normal tissues is not yet understood. This study primarily examines the ROD hypothesis, which posits that oxygen undergoes transient radiolytic depletion following a radiation pulse. We developed a computational model to investigate the effects of dose rate on radiolysis in an aqueous environment that mimics a confined cellular space subjected to instantaneous pulses of energetic protons. This study employed the multi-track chemistry Monte Carlo simulation code, IONLYS-IRT, which has been optimized to model this radiolysis in a homogeneous and aerated medium. This medium is composed primarily of water, alongside carbon-based biological molecules (RH), radiation-induced bio-radicals (R^\bullet), glutathione (GSH), ascorbate (AH^-), nitric oxide ($\bullet NO$), and α -tocopherol (TOH). Our model closely monitors the temporal variations in these components, specifically focusing on oxygen consumption, from the initial picoseconds to one second after exposure. Simulations reveal that cellular oxygen is transiently depleted primarily through its reaction with R^\bullet radicals, consistent with prior research, but also with glutathione disulfide radical anions ($GSSG^{\bullet -}$) in roughly equal proportions. Notably, we show that, contrary to some reports, the peroxy radicals (ROO^\bullet) formed are not neutralized by recombination reactions. Instead, these radicals are rapidly neutralized by antioxidants present in irradiated cells, with AH^- and $\bullet NO$ proving to be the most effective in preventing the propagation of harmful peroxidation chain reactions. Moreover, our model identifies a critical dose rate threshold below which the FLASH effect, as predicted by the ROD hypothesis, cannot fully manifest. By comparing our findings with existing experimental data, we determine that the ROD hypothesis alone cannot entirely explain the observed FLASH effect. Our findings indicate that antioxidants might significantly contribute to the FLASH effect by mitigating radiation-induced cellular damage and, in turn, enhancing cellular radioprotection. Additionally, our model lends support to the hypothesis that transient oxygen depletion may partially contribute to the FLASH effect observed in radiotherapy. However, our findings indicate that this mechanism alone is insufficient to fully explain the phenomenon, suggesting the involvement of additional mechanisms or factors and warranting further investigation.

Keywords: FLASH radiotherapy (FLASH-RT); cell water radiolysis; high dose rate; peroxy radicals; glutathione; ascorbate; nitric oxide; α -tocopherol; Monte Carlo multi-track



Academic Editor: Alessandra Napolitano

Received: 25 February 2025

Revised: 17 March 2025

Accepted: 27 March 2025

Published: 28 March 2025

Citation: Rabeya, I.; Meesungnoen, J.; Jay-Gerin, J.-P. Oxygen Depletion and the Role of Cellular Antioxidants in FLASH Radiotherapy: Mechanistic Insights from Monte Carlo Radiation-Chemical Modeling. *Antioxidants* **2025**, *14*, 406. <https://doi.org/10.3390/antiox14040406>

Copyright: © 2025 by the authors. Licensee MDPI, Basel, Switzerland. This article is an open access article distributed under the terms and conditions of the Creative Commons Attribution (CC BY) license (<https://creativecommons.org/licenses/by/4.0/>).

chemical modeling; radiation chemical yields (G values); radiolytic oxygen depletion (ROD) hypothesis

1. Introduction

1.1. On the FLASH Effect

Radiation therapy (RT) is a fundamental component of modern cancer treatment, employed in conjunction with surgery, chemotherapy, and immunotherapy. Utilizing ionizing radiation, RT targets and eradicates cancer cells, constituting a vital part of the standard oncological care protocol [1]. Since the introduction of X-rays, RT has seen remarkable technological progress. Innovations such as intensity-modulated RT and stereotactic body RT have significantly improved the precision of radiation delivery to tumors, effectively sparing surrounding healthy tissues from damage. A key challenge in RT is to administer cytotoxic doses of radiation that are potent enough to treat cancer effectively while minimizing the risk of severe acute and chronic side effects in nearby normal tissue. In response to this challenge, clinical radiotherapy has recently shifted its focus towards ultra-high dose rate irradiation, known as FLASH irradiation [2–4], which delivers doses at mean rates exceeding ~40 to 150 gray per second (Gy/s). This innovative approach has been found to markedly reduce adverse effects on healthy tissues while maintaining the anti-tumor efficacy seen with standard (STD) clinical dose rates, which are typically ~0.5 to 5 Gy per minute (i.e., several thousand times slower than FLASH irradiation; see, e.g., [5–21]).

The evidence that FLASH-RT can spare normal tissues, thus challenging long-established principles of classical radiobiology, is supported by multiple preclinical studies [22–24]. These investigations, conducted both *in vitro* and *in vivo*, have involved cell cultures and animal models, primarily employing electron linear accelerators. More recently, the protective benefits of FLASH-RT have been demonstrated using megavoltage photons [25–28], cyclotron-based protons [29–33], helium [34], and carbon ions [35–37], significantly broadening its potential applications.

A landmark turning point in the use of FLASH-RT occurred with the treatment of the first human patient, who had cutaneous lymphoma, using a 5.6 MeV electron FLASH beam. This treatment delivered an instantaneous dose rate of 10^6 – 10^7 Gy/s and resulted in the complete eradication of the tumor mass with minimal toxicity to the surrounding healthy tissue, highlighting the therapeutic potential of FLASH-RT [38,39]. Subsequently, a pioneering first-in-human trial explored the use of FLASH proton therapy for managing painful bone metastases [33]. The outcomes indicated that this novel treatment provided pain relief comparable to STD-RT without inducing any unexpected adverse effects, further confirming the clinical promise of FLASH-RT to enhance cancer treatment protocols while reducing side effects. Although there is considerable excitement surrounding these advancements, the precise molecular mechanisms underlying the sparing of normal tissue and the differential responses of tumor and normal tissues to FLASH-RT remain largely undefined. Understanding these aspects is essential for clinically translating the FLASH effect, and it is the primary focus of this study.

Several hypotheses have been proposed to explain the mechanisms underlying the FLASH effect. Among the most notable are the oxygen depletion hypothesis, the reactive oxygen species (ROS) and free radical interaction hypothesis, the DNA integrity hypothesis, the mitochondrial hypothesis, and the immune regulation hypothesis. An expanding body of research investigates these mechanisms, with recent review articles offering comprehensive evaluations [13,14,17,21,24]. Notably, these mechanisms may be interconnected, reflecting the intricate cellular and molecular biology that underlies the FLASH effect [21].

The oxygen depletion hypothesis, also known as the ROD hypothesis [5,40–47], is widely regarded as the most prominent, proposing that the FLASH effect arises, at least in part, from the transient radiolytic consumption or “depletion” of intracellular oxygen. First proposed nearly half a century ago based on experiments with cells irradiated at ultra-high dose rates [48–51], the ROD hypothesis posits that oxygen consumed during a brief period of radiation exposure cannot be replenished quickly enough through diffusion from blood vessels to individual cells. This leads to a temporary state of acute hypoxia, which in turn temporarily enhances the cells’ resistance to radiation. This phenomenon, characterized by decreased radiosensitivity, occurs selectively in oxygenated normal cells, but is absent in tumor cells, which already exist in a poorly oxygenated environment. Despite its widespread acceptance, the ROD hypothesis continues to be debated [52–55], specifically concerning whether the amount of O₂ depleted during pulse irradiation is enough to induce significant hypoxia in initially well-oxygenated tissues *in vivo*, thereby fully accounting for the protective effects observed with FLASH-RT.

Our work is mainly focused on the first two hypotheses which are based mainly on chemical reactions between primary products formed during water radiolysis and either oxygen and/or biological molecules and endogenous antioxidants.

1.2. Water Radiolysis in Cellular Environments

Water is the primary component in living cells and tissues by weight, making an understanding of water radiolysis essential for comprehending radiobiological effects. Quantitatively, the main products of the radiolysis of pure deaerated water include hydrated electrons (e^-_{aq}), hydrogen atoms (H^\bullet), molecular hydrogen (H₂), hydroxyl radicals ($^\bullet OH$), hydrogen peroxide (H₂O₂), hydronium ions (H₃O⁺), and hydroxide ions (OH[−]) (see, e.g., [56–59]). These products initially form within a nonhomogeneous track structure where $^\bullet OH$ and e^-_{aq} radicals are most abundant. Under aerated conditions, e^-_{aq} and H^\bullet atoms quickly (within microseconds) convert to superoxide/hydroperoxyl radicals (O₂ $^{\bullet -}$ /HO₂ $^\bullet$), with O₂ $^{\bullet -}$ in pH-dependent equilibrium with its conjugate acid (pK_a ≈ 4.8 at 25 °C) [60]. As a result, at physiological pH, the main reactive species when homogeneity is achieved are O₂ $^{\bullet -}$, $^\bullet OH$, and H₂O₂. H₂ plays only a minor role in the radiolysis of aqueous solutions, with most of it escaping from the solution.

In cellular environments, the situation is markedly different. Firstly, while reactions involving e^-_{aq} and H^\bullet with O₂ are prominent in pure, aerated water radiolysis, they are much less frequent in cells. This reduction is largely due to the high concentration of intracellular bio-organic molecules (collectively referred to as RH), such as DNA, proteins, and lipids [47,61–63], which effectively compete with O₂ for the capture of these species [40,47,62–67]. For instance, the scavenging power for the reaction of e^-_{aq} with these biomolecules is estimated to be $3.4 \times 10^8 \text{ s}^{-1}$ [61], nearly 1000 times greater than that for 30 μM oxygen—a typical concentration in most normal tissues [56]—estimated at $5.7 \times 10^5 \text{ s}^{-1}$. Here, “scavenging power” refers to the product of the scavenger’s concentration and its reaction rate constant with e^-_{aq} . This notable difference in scavenging power between cellular components and oxygen within cells was underscored by Wardman [64] and Favaudon et al. [47], and further substantiated through Monte Carlo multi-track chemistry simulations by Sultana et al. [68]. This challenges the previous model of treating a cell merely as a “bag” of pure, aerated water (see, e.g., [69–73]). Indeed, during FLASH irradiation, the temporary depletion of O₂ by e^-_{aq} /H $^\bullet$ is very low in a cellular or tissue environment.

Secondly, in irradiated biological systems, carbon-centered organic radicals (represented by R $^\bullet$) are generated through two main pathways: the deprotonation of intermediate radical cations (RH $^{\bullet +}$) that initially arise from the direct ionization of biomolecules or via

hydrogen abstraction reactions involving RH. The latter pathway commonly involves $\bullet\text{OH}$ radicals produced through the radiolysis of water [56,57,74]:



The rate constant for this reaction typically ranges from 10^8 to $10^9 \text{ M}^{-1} \text{ s}^{-1}$, influenced by the specific structure of RH and the type of hydrogen atoms it contains. Under oxidative stress, if cellular antioxidant defenses like glutathione, vitamin C (ascorbate), or vitamin E (α -tocopherol)—which donate hydrogen atoms to repair molecular damage—are inadequate, $\text{R}\bullet$ radicals can react with O_2 to produce peroxy radicals ($\text{ROO}\bullet$). These reactions occur at rates approaching the diffusion-controlled limit [75–78]:



Peroxy radicals are more potent oxidizers than their precursor radicals. As chain-propagating species, they particularly target polyunsaturated lipids from which they abstract $\text{H}\bullet$ atoms, leading to hydroperoxide (ROOH) formation—a key step in lipid peroxidation processes [75,79–82]. These $\text{ROO}\bullet$ radicals can also form in various cellular macromolecules, including proteins and DNA (see, e.g., [83]). Once generated, peroxy radicals permanently alter the original molecules, a process known as the “fixation” of damage by oxygen [84,85]. This irreversible damage presents formidable obstacles for cellular repair mechanisms, often making the restoration of damaged structures challenging or unachievable.

In other words, the physiological levels of oxygen and antioxidants are pivotal in shaping the outcomes for intermediate radicals in biomolecules. Labarbe et al. [47,62] emphasized that any cellular processes which either reduce the radiolytic production of $\text{ROO}\bullet$ radicals or shorten their lifetime could protect healthy tissues from the detrimental effects of radiation. This insight prompted these authors [47] and others [64–66] to suggest that radical–radical combination and recombination ($\text{ROO}\bullet\text{-ROO}\bullet$, $\text{ROO}\bullet\text{-R}\bullet$, or $\text{R}\bullet\text{-R}\bullet$) could account for the protective effects seen with FLASH irradiation, a hypothesis supported by the high dose rates characteristic of FLASH-RT. From a radiation–chemical perspective, high dose rate irradiation increases transient radical concentrations through enhanced multi-track chemistry [57,86,87], potentially raising the proportion of peroxy radical recombination during FLASH irradiation relative to STD-RT. However, contrary to these expectations, the model presented here indicates that such recombination reactions have minimal impact on outcomes within the first second after irradiation. Comparable findings were also reported by Baikalov et al. [88]. This limited effect is partly due to the relatively slow nature of these reactions, with rate constants ranging from $\sim 10^4 \text{ M}^{-1} \text{ s}^{-1}$ for ($\text{ROO}\bullet + \text{ROO}\bullet$) to $\sim 10^8 \text{ M}^{-1} \text{ s}^{-1}$ for ($\text{R}\bullet + \text{R}\bullet$).

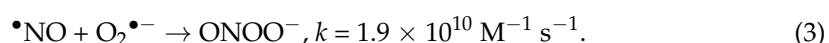
1.3. Investigating the Role of Cellular Antioxidants in FLASH-RT

Building on these findings and Wardman’s discussions [64], we propose that cellular antioxidants, rather than $\text{ROO}\bullet$ and $\text{R}\bullet$ radical–radical recombination reactions, are central to mediating the FLASH radiotherapeutic response. The antioxidants considered in this study include nitric oxide ($\bullet\text{NO}$, also known as nitrogen monoxide), glutathione (GSH), ascorbate (AH^-), and α -tocopherol (TOH). Below, we explore the significance and relevance of each of these antioxidants in addressing the problem at hand.

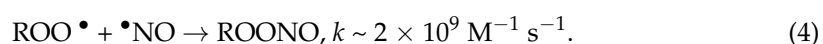
(1) $\bullet\text{NO}$, a naturally occurring free radical (note that the unpaired electron is located on the nitrogen atom) produced endogenously in most mammalian cells, is synthesized by a family of enzymes known as nitric oxide synthases (NOS), which are divided into constitutive (cNOS) and inducible (iNOS) isoforms. Particularly pertinent to our research,

iNOS can be activated by inflammatory stimuli like physiological stress, often triggered by events that generate excessive reactive oxygen/nitrogen species (ROS/RNS) such as those occurring during high dose rate (FLASH) irradiation. This leads to the production of $\bullet\text{NO}$ in supraphysiological concentrations, potentially reaching micromolar levels or sustained over extended periods of time (see, e.g., [82,89–94] and cited references). This increased $\bullet\text{NO}$ production can be viewed as a protective or adaptive response, where $\bullet\text{NO}$ acts as an antioxidant by scavenging free radicals produced by radiation, thereby reducing oxidative stress and potentially minimizing DNA damage.

However, in the presence of superoxide radicals ($\text{O}_2^{\bullet-}$), $\bullet\text{NO}$ can also contribute to cytotoxic effects by generating highly reactive peroxynitrite (ONOO^- , $\text{pK}_a = 6.8$ at 37°C) [92,95–97]:



Moreover, nitric oxide is involved in one of the fastest known reactions with organic peroxy radicals, resulting in the formation of organic peroxynitrites (or pernitrites) [76,82,98–100]:



Organic peroxynitrites are generally unstable and likely non-reactive. In fact, ROONO may undergo the homolytic cleavage of the O–O bond, resulting in a caged radical pair that can either recombine to form a more stable organic nitrate, RONO_2 , or dissociate into free alkoxy (RO^\bullet) and nitrogen dioxide ($\bullet\text{NO}_2$) radicals. This dissociation pathway could theoretically increase lipid peroxidation, a process that contradicts numerous studies underscoring $\bullet\text{NO}$'s antioxidant properties [99–101]. However, it has been suggested that RO^\bullet could react with $\bullet\text{NO}$ to give RONO , thus inhibiting further oxidative reactions. Moreover, $\bullet\text{NO}_2$ can react with $\bullet\text{NO}$ to form dinitrogen trioxide, which subsequently hydrolyzes to nitrite anion [99].

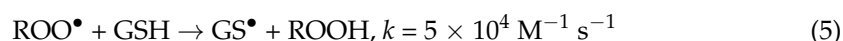
Due to its high lipophilicity, charge neutrality, and small molecular size, $\bullet\text{NO}$ easily diffuses through cell membranes and accumulates in lipophilic compartments. It acts as an effective lipid-soluble, chain-breaking antioxidant, not only inhibiting lipid peroxidation propagation but also preserving lipophilic antioxidants, such as α -tocopherol [102], thereby enhancing the overall cellular resistance to radiation. Notably, in FLASH-irradiated cells, reaction (4) predominates over reaction (3) because O_2 is more likely to be consumed in forming ROO^\bullet rather than reacting with e^-_{aq} or H^\bullet to form $\text{O}_2^{\bullet-}$, due to the high concentrations of competing intracellular scavengers for $\text{e}^-_{\text{aq}}/\text{H}^\bullet$, as previously discussed [64,68].

These rapid reactions between peroxy radicals and $\bullet\text{NO}$ are critical in regulating lipid oxidation processes in cell membranes, lipoproteins, and other lipid-containing structures, which are central to this study. These reactions are particularly significant for their potential contribution to the FLASH effect, where $\bullet\text{NO}$'s antioxidant capabilities could play a crucial role in synergy with other key cellular antioxidants like glutathione, ascorbate, and α -tocopherol.

In this study, a nitric oxide concentration of $[\bullet\text{NO}] = 1 \mu\text{M}$ was used. As previously mentioned, this concentration exceeds the estimated steady-state $\bullet\text{NO}$ levels in normal tissue, which typically range from ~ 0.02 to $0.1 \mu\text{M}$, reflecting the specific conditions associated with the high dose rate effects of FLASH irradiation [82,89–94,103,104].

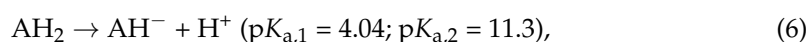
(2) Thiols are well-known for their role in protecting cells from damage caused by ROS/RNS [75,82]. In this study, we selected glutathione (GSH) as the representative thiol antioxidant because of its high prevalence in mammalian tissues, where it is commonly found at millimolar concentrations (1–10 mM) [105]. Although GSH is primarily synthe-

sized in the cytoplasm, it is also abundant in the cell nucleus. Notably, GSH exhibits moderate reactivity with ROO• peroxy radicals, leading to the formation of the glutathione thiyl radical GS• [77,106]:

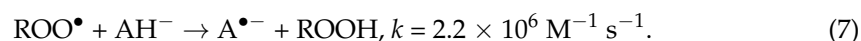


This radical can further react with O₂, •NO, and ascorbate (AH[−]) or dimerize to produce the oxidized form of glutathione, glutathione disulfide (GSSG) (see, e.g., [82]). To simulate the intracellular environment in our cellular model, we used a concentration of [GSH] = 6.5 mM. This concentration aligns with the values reported in the existing literature [62,65,67,105,107,108], highlighting GSH's critical role in mitigating oxidative stress and maintaining the cellular redox balance.

(3) Ascorbic acid (vitamin C, AH₂), along with glutathione, is a potent water-soluble biological antioxidant and free-radical scavenger. It is typically present in most cells at relatively high concentrations, ranging from 1 to 2.5 mM [109,110]. Ascorbic acid readily loses a proton to form the ascorbate anion [111,112]:



making the protonated form negligible at physiological pH. Ascorbate anions react with ROO• according to [63,76,77,109]:



Ascorbate radicals (A^{•−}), also known as ascorbyl radicals, generated in reaction (7), are relatively unreactive. They primarily undergo disproportionation among themselves, serving as effective free radical chain terminators [113–115]. Importantly, A^{•−} does not readily engage in addition reactions with O₂ ($k < 5 \times 10^2 \text{ M}^{-1} \text{ s}^{-1}$), thus preventing the formation of harmful peroxy radicals [115,116]. Similarly, these radicals exhibit minimal reactivity with •NO [110]. In our simulations, we employed an ascorbate concentration of [AH[−]] = 1 mM.

(4) Vitamin E is recognized as the first and most potent lipid-soluble chain-breaking antioxidant [117]. α-tocopherol (TOH) is known to react with peroxy radicals within lipid-rich environments, such as membranes or lipoproteins, effectively preventing lipid peroxidation. Remarkably, the tocopheroxy radicals (TO•) produced in this reaction can be regenerated into functional vitamin E by ascorbate (AH[−]), thereby providing sustained antioxidant protection [82,101,114,118,119]. Furthermore, note that there is no direct reaction between nitric oxide and TO• radicals [101]. For our simulations, we utilized an α-tocopherol concentration of [TOH] = 0.2 mM [65].

2. Materials and Methods

2.1. Determining the Effects of Dose Rates Using the ‘Instantaneous Pulse’ (Dirac) Model

In this study, we employed our newly developed multi-track irradiation model to explore the impact of high dose rates on water radiolysis using single, instantaneous pulses of *N* incident 300-MeV protons [68,69,87,120]. These protons mimic the low linear energy transfer (LET) characteristic of ⁶⁰Co γ-ray Compton electrons or fast (e.g., MeV) electrons, with an LET of ~0.3 keV/μm [121]. Notably, in the absence of dose rate effects (i.e., no interaction between tracks), their track structure initially comprises small, well-separated Magee-type “spurs”—roughly spherical clusters of radiolytic species distributed along the radiation path [57–59]).

Briefly, these monoenergetic protons simultaneously strike the water surface perpendicularly, covering a circular area with radius R_0 , as illustrated in Figure 1 of Alanazi et al. [69]. Known as the ‘instantaneous pulse’ or Dirac model, this method assumes a pulse duration of zero [122], leading to the immediate formation of all chemical species.

Using energetic protons offers the advantage of their essentially rectilinear trajectories, allowing the definition of a cylindrical beam geometry upon entry. Within this configuration, all proton tracks are aligned with the cylinder’s axis for the entire chosen track length. This setup closely mirrors the conditions encountered in our long-standing Monte Carlo simulations of water radiolysis at low dose rates (see, e.g., [59] for a review), but instead of simulating a single proton track, we simultaneously simulate N interactive tracks. In this particular setup, the incident proton “fluence” (number of impacting protons per unit area) is calculated as $N/\pi R_0^2$.

By varying N , the number of protons per pulse, we directly investigate how different dose rates affect our system. This study examines four values of N : 20, 30, 40, and 50. Based on our prior calibration of N in relation to dose rate (refer to Figure 3B in Alanazi et al. [69]), $N = 20$ corresponds to an absorbed dose rate of $\sim 10^6$ – 10^7 Gy/s under our irradiation conditions.

We define “time zero” as the moment the N incident protons reach the front of the cylinder.

2.2. Monte Carlo Multi-Track Chemistry Simulations Using the IONLYS-IRT Code

In the context of water radiolysis, our IONLYS program [59,123] simulates the initial physical and physicochemical stages of radiation action within a 3D environment, capturing events up to ~ 1 picosecond (ps) in track development. It accurately models each event, detailing all fundamental physical interactions associated with energy deposition and the transformation of local physical products into various initial radical and molecular radiolysis products. These products include e^-_{aq} , H^\bullet , H_2 , $\bullet OH$, H_2O_2 , H^+ , and OH^- , among others [59]. This program generates a detailed and highly nonhomogeneous spatial distribution of reactants, setting the stage for the subsequent chemical stage of radiolysis that begins after ~ 1 ps. In this third stage, the various radiolytic products diffuse randomly from their origin points, governed by their diffusion coefficients. They react either with each other or, competitively, with uniformly distributed solutes in the system. Our IRT program [124] handles this stage using the “independent reaction times” (IRT) method [125–127], a stochastic simulation technique that efficiently calculates reaction times without needing to track individual diffusion trajectories. The accuracy of this program in delivering chemical yields (or G values) has been validated under various irradiation conditions through comparisons with detailed “step-by-step” Monte Carlo simulations, which closely track the trajectories of diffusing reactive species [128]. Additionally, the IRT program is particularly effective in modeling reactions over extended periods of time when tracks have dissipated and the radiolytic products are uniformly distributed within the solution.

Throughout this article, G values are expressed as the number of molecules formed or consumed per 100 eV of absorbed radiation energy. The conversion of these values to SI units is as follows: 1 molecule per 100 eV ≈ 0.103364 $\mu\text{mol/J}$ [57].

2.3. Our Irradiated Cell Water Model: Proposed Chemical Reaction Scheme

In our approach, we model a cell as a homogeneous aqueous medium, thereby ignoring cellular heterogeneity. Cells are inherently complex, consisting of various compartments and structures like the cytoplasm, nucleus, mitochondria, and phospholipid membranes, each characterized by unique chemical and physical properties. As pointed out by Ward-

man [63,64,129], while homogeneous kinetics provide a practical modeling framework, this approach may overlook important aspects of cellular behavior and interactions. Despite these limitations, we argue that our basic cell water model, which utilizes homogeneous kinetics, is instrumental for identifying primary reactants and key reactions in cells exposed to high dose rates, thus advancing our understanding of the chemical mechanisms driving the FLASH effect.

The model assumes cellular composition based on the following:

- Dissolved oxygen, typically around 30 μM in well-oxygenated mammalian tissues, as reported in [56,68,103].
- Carbon-based biomolecules (RH), such as DNA and RNA (present in much lower concentrations than proteins and lipids), proteins (the primary components by weight in most cells), free amino acids, free nucleotides, and lipids (mainly in cell membranes), typically occur at a concentration of $[\text{RH}] \sim 1 \text{ M}$ [62,130]. This concentration has been previously utilized in the literature (e.g., see [62,67]). In our simulations, 1 M denotes the ‘oxidizable’ substrate concentration in a living system, as defined by Qian and Buettner [130]. Nevertheless, a 1 M concentration of bio-organic molecules may appear high when averaged across an entire cell. To account for some cellular heterogeneity, we also tested a 0.5 M concentration, both for comparison and to evaluate the sensitivity of the results to $[\text{RH}]$ variations.
- For simplicity, as noted above, our model does not distinguish between these macromolecular constituents. We acknowledge that using a single RH species poorly captures variations in radiation-induced cellular damage, particularly the differences between DNA and lipids. To improve accuracy, we are currently developing a more detailed compartmental cell model akin to those proposed by Hu et al. [65] and Babbs and Steiner [106].
- Under the specific conditions of FLASH irradiation employed in this study—a $\sim 30 \text{ Gy}$ dose delivered with 300-MeV protons ($\text{LET} \sim 0.3 \text{ keV}/\mu\text{m}$) at an instantaneous dose rate of $\sim 10^6\text{--}10^7 \text{ Gy/s}$ [68,69]—we estimate an initial bio-radical (R^\bullet) concentration of $\sim 2.5 \mu\text{M}$. These bio-radicals originate from the ‘direct’ ionization of RH, followed by the deprotonation of the resulting radical cations ($\text{RH}^{\bullet+}$). This concentration estimate is derived from direct action yields reported in previous studies [40,62,65].

We supplemented the reaction scheme in our IONLYS-IRT track chemistry computer code, which models the radiolysis of pure, deaerated liquid water at 25°C under 300-MeV proton irradiation (refer to Table 14.1 in [59])—a condition that mimics cobalt-60 γ -ray exposure (as previously discussed) to incorporate 48 reactions relevant to the irradiated cell water model being studied. These specific reactions are listed in Table 1.

Table 1. Reaction scheme and rate constants (k , in $\text{M}^{-1} \text{s}^{-1}$) for simulating radiolysis of our cell water model at room temperature ^{a,b}.

Symbol	Reaction	k	References
(R1)	$\text{RH} + \text{e}^-_{\text{aq}} \rightarrow (\text{RH})^{\bullet-}$	1.5×10^9	[61,131,132]
(R2)	$\text{RH} + \text{H}^\bullet \rightarrow \text{RH}(+\text{H})^\bullet$	8×10^7	[61,131–133]
(R3)	$\text{O}_2 + \text{e}^-_{\text{aq}} \rightarrow \text{O}_2^{\bullet-}$	1.9×10^{10}	[74]
(R4)	$\text{O}_2 + \text{H}^\bullet \rightarrow \text{HO}_2^\bullet \rightarrow \text{O}_2^{\bullet-} + \text{H}^+ \text{ (pK}_a = 4.8) \text{ }^c$	2.1×10^{10}	[60,74]
(R5)	$\text{O}_2^{\bullet-} + \text{O}_2^{\bullet-} + 2\text{H}^+ \rightarrow \text{O}_2 + \text{H}_2\text{O}_2 \text{ }^d$	4×10^9	[82,92,134]
(R6)	$\text{H}_2\text{O}_2 + \text{H}_2\text{O}_2 \rightarrow 2\text{H}_2\text{O} + \text{O}_2 \text{ }^e$	2×10^7	[82]
(1)	$\text{RH} + \bullet\text{OH} \rightarrow \text{R}^\bullet + \text{H}_2\text{O}$	5×10^8	[56,57,61,74,132]
(2)	$\text{R}^\bullet + \text{O}_2 \rightarrow \text{ROO}^\bullet$	2×10^9	[75–78]

Table 1. Cont.

Symbol	Reaction	k	References
(R7)	$R^\bullet + R^\bullet \rightarrow R-R$	10^8	[62,106]
(R8)	$R^\bullet + ROO^\bullet \rightarrow ROOR$	5×10^7	[106]
(R9)	$ROO^\bullet + ROO^\bullet \rightarrow \text{products}$	10^5	[62,65,75]
(R10)	$ROO^\bullet + RH \rightarrow ROOH + R^\bullet$	1.3×10^3	[62,65,75]
(R11)	$ROO^\bullet + O_2^{\bullet-} + H^+ \rightarrow ROOH + O_2$	5×10^7	[82,106,135]
(R12)	$e^-_{aq} + ROOH \rightarrow RO^\bullet + OH^-$	10^{10}	[56]
(R13)	$RO^\bullet + RH \rightarrow ROH + R^\bullet$	5×10^{4f}	[57]
(5)	$ROO^\bullet + GSH \rightarrow GS^\bullet + ROOH^g$	5×10^4	[77,106]
(R14)	$R^\bullet + GSH \rightarrow GS^\bullet + RH$	5.6×10^6	[65]
(R15)	$GSH + e^-_{aq} + H^+ \rightarrow G^\bullet + H_2S$	4.5×10^9	[74]
(R16)	$GSH + H^\bullet \rightarrow GS^\bullet + H_2^h$	1.8×10^9	[136]
(R17)	$GSH + \bullet OH \rightarrow GS^\bullet + H_2O$	1.4×10^{10}	[74,106,137,138]
(R18)	$GS^\bullet + O_2 \rightarrow GSOO^\bullet$	2×10^9	[65,139–141]
(R19)	$GSOO^\bullet \rightarrow GS^\bullet + O_2$	6.2×10^5	[65,108,130]
(R20)	$GSOO^\bullet + GSH \rightarrow GSO^\bullet + GSOH$	2×10^6	[108]
(R21)	$GS^\bullet + GS^\bullet \rightarrow GSSG^i$	7.5×10^8	[82,139,142]
(R22)	$GS^\bullet + GSH \rightarrow GSSG^{\bullet-} + H^+$	3.5×10^8	[65,136,137,142]
(R23)	$GSSG^{\bullet-} + O_2 \rightarrow GSSG + O_2^{\bullet-}$	5.1×10^8	[82,139–141]
(R24)	$GSSG + e^-_{aq} \rightarrow GSSG^{\bullet-}$	3.7×10^9	[74]
(R25)	$GSSG + H^\bullet \rightarrow GSH + GS^\bullet$	10^{10}	[74]
(R26)	$GSSG + \bullet OH \rightarrow GSSG^{\bullet+} + OH^-$	1.7×10^{10}	[136]
(R27)	$GSSG^{\bullet+} + GSSG^{\bullet+} \rightarrow GSSG^{2+} + GSSG$	2.5×10^9	[136]
(R28)	$GS^\bullet + \bullet NO \rightarrow GSNO$	3×10^9	[142]
(R29)	$GS^\bullet + GSNO \rightarrow GSSG + \bullet NO$	1.7×10^9	[142]
(R30)	$GS^\bullet + AH^- \rightarrow GSH + A^{\bullet-}{}^{j,k}$	6×10^8	[65,82,139,140]
(R31)	$R^\bullet + AH^- \rightarrow RH + A^{\bullet-}$	10^7	[65]
(7)	$ROO^\bullet + AH^- \rightarrow ROOH + A^{\bullet-}$	2.2×10^6	[63,76,77,109,113–115]
(R32)	$RO^\bullet + AH^- \rightarrow ROH + A^{\bullet-}$	1.6×10^9	[114,115]
(R33)	$AH^- + O_2^{\bullet-} + H^+ \rightarrow A^{\bullet-} + H_2O_2$	2.7×10^5	[82,114–116,139]
(R34)	$AH^- + \bullet OH \rightarrow A^{\bullet-} + H_2O$	1.1×10^{10}	[74,82,114,115]
(R35)	$A^{\bullet-} + A^{\bullet-} + H^+ \rightarrow AH^- + A^l$	2.8×10^5	[113–115]
(R36)	$A^{\bullet-} + O_2^{\bullet-} + 2H^+ \rightarrow A + H_2O_2$	2.6×10^8	[113,114]
(R37)	$\bullet OH + TOH \rightarrow TO^\bullet + H_2O^m$	10^{10}	[106]
(R38)	$R^\bullet + TOH \rightarrow RH + TO^\bullet$	2.5×10^6	[65,106]
(R39)	$ROO^\bullet + TOH \rightarrow ROOH + TO^\bullet$	5×10^5	[56,65,82,99,101,106]
(R40)	$TO^\bullet + AH^- \rightarrow TOH + A^{\bullet-}$	1.3×10^7	[114]
(3)	$NO^\bullet + O_2^{\bullet-} \rightarrow ONOO^{\bullet-}{}^n$	1.9×10^{10}	[95–98,143–145]
(R41)	$NO^\bullet + \bullet OH \rightarrow HNO_2$	10^{10}	[82]
(R42)	$R^\bullet + \bullet NO \rightarrow RNO$	2×10^9	[129]
(4)	$ROO^\bullet + \bullet NO \rightarrow ROONO$	$2 \times 10^9{}^o$	[98–102]

^a The rate constants quoted here for reactions between ions are based on conditions of infinite dilution, where ion–ion interactions are absent. In the IRT program, we disregarded the effects of ionic strength on all these reactions.

^b For the model presented here, much of the chemistry is well established. However, there are uncertainties associated with the reaction rate constants. These uncertainties can vary significantly, ranging from a few percent to a factor of ten or more in some instances. ^c Favored at physiological pH. ^d Enzymatic dismutation of $O_2^{\bullet-}$ catalyzed by Cu/Zn superoxide dismutase (SOD). ^e In the presence of catalase. ^f Estimated from [57]. ^g GS^{\bullet} : Glutathione thiyl radical. ^h Assuming that the rate constant for this reaction is similar to the rate at which H^{\bullet} atoms react with cysteine (CysSH) in aqueous solution ($k \sim 1\text{--}4 \times 10^9 \text{ M}^{-1} \text{ s}^{-1}$) (refer to Table 2 in [136]). ⁱ GSSG: Glutathione disulfide, also commonly referred to as oxidized glutathione. ^j AH^- : Monohydrogen ascorbate anion. ^k $A^{\bullet-}$: Ascorbate or ascorbyl radicals. ^l Dehydroascorbic acid (A) produced by the disproportionation of two ascorbate radicals. ^m TO^{\bullet} : Tocopheroxyl radical. ⁿ $ONOO^-$: peroxynitrite. ^o Nitric oxide is $10^4\text{--}10^5$ times more effective as a peroxyl radical scavenger than α -tocopherol [99].

3. Results and Discussion

To clarify the molecular mechanisms underlying radiolysis in our modeled bulk cell water described above, Figure 1 presents the time profiles of the yields of the key chemical species involved in the process. As can be seen, carbon-centered free radicals (R^{\bullet}) and peroxy radicals (ROO^{\bullet}) are primarily produced, with R^{\bullet} forming via reaction (1) and ROO^{\bullet} via reaction (2) during oxygen consumption. Conversely, cellular biomolecules (RH) and oxygen are primarily consumed (“depleted”) through reactions (1) and (R1) and reaction (2), respectively. These findings underscore the dominant role of R^{\bullet} in O_2 consumption within the 1–100 μs range. Figure 2a,b reinforces this by displaying the time-dependent extents $\Delta G(R^{\bullet})$ and $\Delta G(ROO^{\bullet})$, expressed as molecules per 100 eV, for each reaction contributing to $G(R^{\bullet})$ and $G(ROO^{\bullet})$ from 1 ps to 1 s, based on our Monte Carlo simulations.

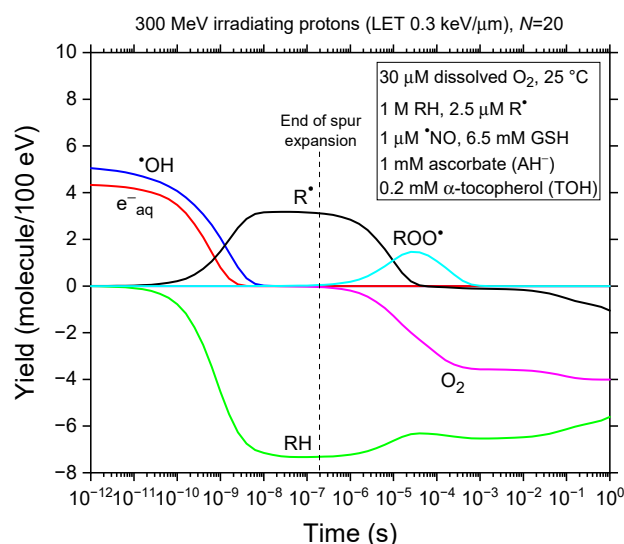


Figure 1. Time evolution of the yields of key reactive species (e^-_{aq} , $^{\bullet}OH$, RH, R^{\bullet} , ROO^{\bullet} , and O_2) from our IONLYS-IRT Monte Carlo track chemistry simulations of radiolysis in our modeled cell-like water, which contains 30 μM dissolved oxygen at 25 $^{\circ}\text{C}$, covering a time span from 1 ps to 1 s. Simulations were conducted under representative FLASH irradiation conditions using 300-MeV incident protons ($LET \sim 0.3 \text{ keV}/\mu\text{m}$), delivering $\sim 30 \text{ Gy}$ at an instantaneous dose rate of $\sim 10^6\text{--}10^7 \text{ Gy/s}$, corresponding to $N = 20$ irradiating protons per pulse. For reference, the dashed line at $\sim 0.2 \mu\text{s}$ indicates the transition from nonhomogeneous spur kinetics to homogeneous kinetics in the bulk solution in the absence of dose rate effects [57,146].

Figure 2a reveals that glutathione (GSH) and ascorbate (AH^-) also contribute to R^{\bullet} removal in this time range, though less efficiently. Figure 2b illustrates the role of cellular antioxidants in scavenging ROO^{\bullet} radicals, with ascorbate and nitric oxide ($^{\bullet}NO$) being the most effective, while GSH and α -tocopherol (TOH) play minor roles. Efficient scavenging between 10 μs and $\sim 1 \text{ ms}$ underpins the bell-shaped $G(ROO^{\bullet})$ curve, peaking at $\sim 50 \mu\text{s}$ and disappearing after 1 ms (see Figure 1). This rapid antioxidant response effectively minimizes ROO^{\bullet} -mediated lipid peroxidation, oxidative stress, and DNA damage beyond

the millisecond scale. Ascorbate, $\bullet\text{NO}$, GSH, and TOH act as potent radioprotectors by rapidly neutralizing radiation-induced peroxy radicals, thereby significantly mitigating oxidative damage. These results challenge the findings of Labarbe et al. [47,62], who attributed FLASH radioprotection mainly to radiolytic $\text{ROO}\bullet$ neutralization through $\text{R}\bullet$ and $\text{ROO}\bullet$ radical–radical combination or recombination. Our data indicate that these reactions only have a limited impact due to slower kinetics. Baikarov et al. [88] reached similar conclusions. This, in turn, underscores the critical role of fast-reacting cellular antioxidants, especially ascorbate and nitric oxide, in achieving effective FLASH radioprotection. These antioxidants not only neutralize radiation-induced peroxy radicals quickly but also prevent downstream oxidative damage, thereby maintaining cellular integrity during FLASH irradiation.

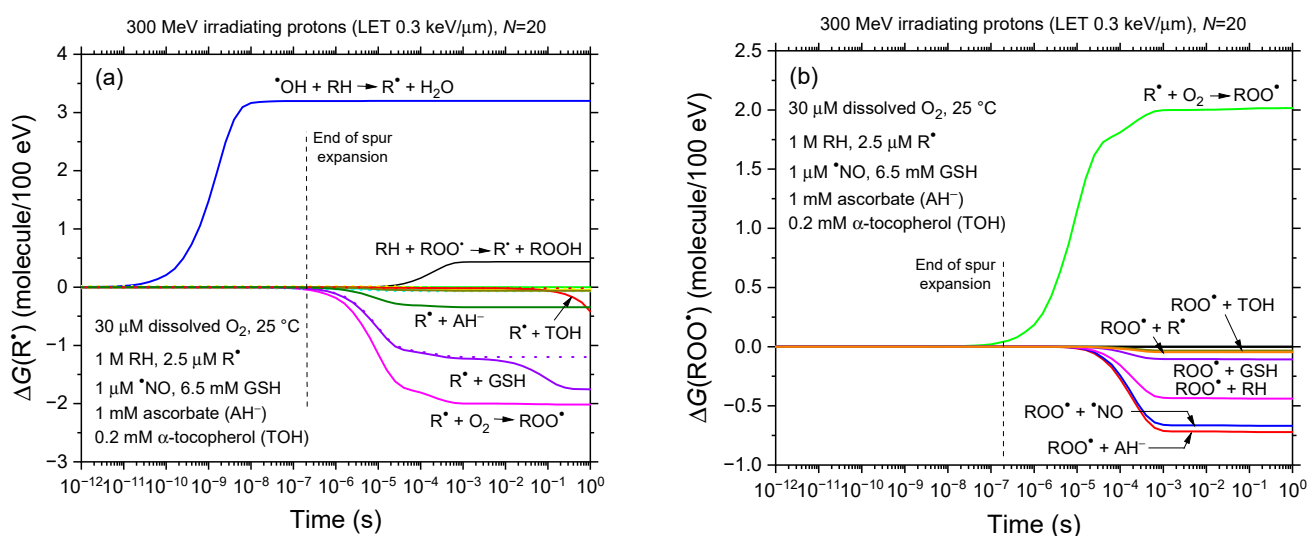


Figure 2. Time-dependent extents $\Delta G(\text{R}\bullet)$ (panel a) and $\Delta G(\text{ROO}\bullet)$ (panel b), expressed in molecules per 100 eV, for various reactions contributing to $G(\text{R}\bullet)$ and $G(\text{ROO}\bullet)$ (shown in Figure 1) from 1 ps to 1 s, based on our Monte Carlo simulations. The irradiation conditions are the same as those described in the caption of Figure 1. Panel (a) shows that $\text{R}\bullet$ primarily forms at early times through reaction (1) ($\text{RH} + \bullet\text{OH} \rightarrow \text{R}\bullet + \text{H}_2\text{O}$) and, much later and to a significantly lesser extent, through reaction (R10) ($\text{RH} + \text{ROO}\bullet \rightarrow \text{R}\bullet + \text{ROOH}$). Its consumption after approximately a microsecond, mainly through reactions with O_2 and GSH, with smaller contributions from ascorbate (AH^-) and α -tocopherol (TOH). The two dotted lines depict the contributions of reactions (R14) ($\text{R}\bullet + \text{GSH} \rightarrow \text{GS}\bullet + \text{RH}$) and (R38) ($\text{R}\bullet + \text{TOH} \rightarrow \text{TO}\bullet + \text{RH}$), assuming the absence of $\text{R}\bullet$ from the ‘direct’ ionization of RH. As observed, the initial bio-radical $\text{R}\bullet$ concentration of 2.5 μM, as utilized in this study, only becomes significant at times exceeding ~10 ms; panel (b) indicates that $\text{ROO}\bullet$ is primarily formed on the microsecond timescale via reaction (2) ($\text{R}\bullet + \text{O}_2 \rightarrow \text{ROO}\bullet$). Its consumption, occurring after tens of microseconds, is largely driven by reactions with ascorbate and nitric oxide ($\bullet\text{NO}$), with reactions involving GSH and TOH playing a minor role. For reference, the dashed line at ~0.2 μs marks the transition from nonhomogeneous spur kinetics to homogeneous kinetics in the absence of dose rate effects.

Figure 3a presents the time evolution of the oxygen consumption yield, $G(-\text{O}_2)$, during the radiolysis of our modeled cell-like water containing 30 μM dissolved oxygen at 25 °C, over a timescale from 1 ps to 1 s. Figure 3b provides a detailed breakdown of the time-dependent contributions, $\Delta G(-\text{O}_2)$, of individual reactions to $G(-\text{O}_2)$, based on our Monte Carlo simulations. As expected, $G(-\text{O}_2)$ remains at zero during the first moments since O_2 is not a primary species in low-LET water radiolysis. However, it begins to increase once dissolved O_2 reacts with $\text{R}\bullet$ and $\text{GSSG}^{\bullet-}$ (glutathione disulfide radical anion) via reactions (2) and (R23). In this process, $G(-\text{O}_2)$ rises rapidly, reaching a plateau of about 4G units

around 1 s. Notably, the involvement of reaction (R23) ($\text{GSSG}^{\bullet-} + \text{O}_2 \rightarrow \text{GSSG} + \text{O}_2^{\bullet-}$) in oxygen depletion has not been previously recognized; its contribution, nearly 2G units at ~ 1 s, is comparable to that of reaction (2). In contrast, reaction (R18) ($\text{GS}^{\bullet} + \text{O}_2 \rightarrow \text{GSOO}^{\bullet}$) has a negligible impact.

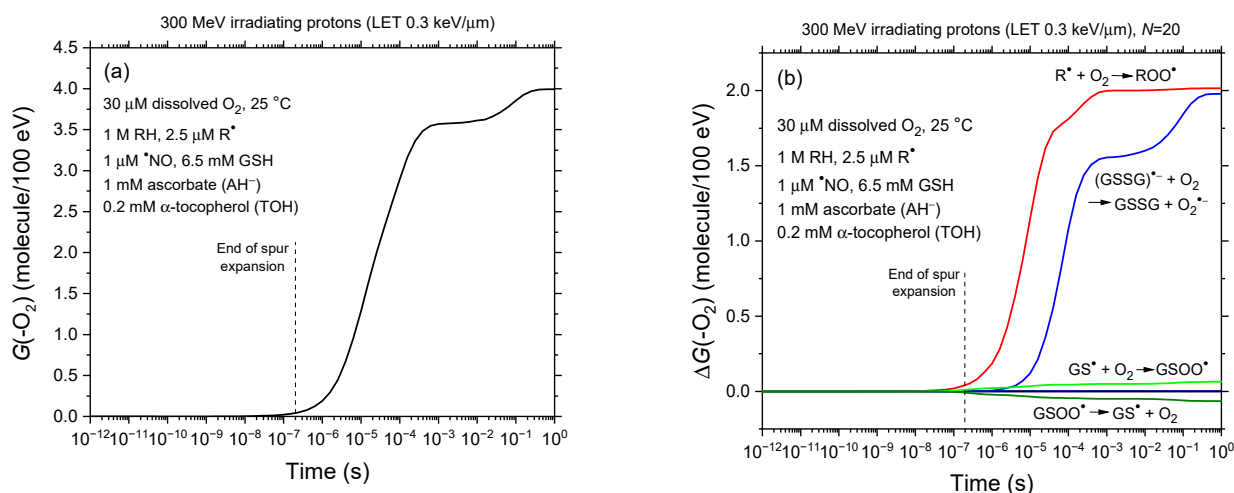


Figure 3. Panel (a): Time evolution of the oxygen consumption yield, $G(-\text{O}_2)$, obtained from our IONLYS-IRT Monte Carlo track chemistry simulations of radiolysis in our modeled cell-like water containing 30 μM dissolved oxygen at 25 °C. The simulations covered timescales from 1 ps to 1 s, employing 300-MeV incident protons (LET ~ 0.3 keV/μm) at various dose rates, each pulse involving 20 to 50 irradiating protons. The resulting $G(-\text{O}_2)$ -vs.-time curves remain nearly superimposed independent of the value of N (see text). Panel (b): Time-dependent extents $\Delta G(-\text{O}_2)$, expressed in molecules per 100 eV, for the individual reactions contributing to $G(-\text{O}_2)$ from 1 ps to 1 s, based on our Monte Carlo simulations. Oxygen consumption primarily occurs through reactions with R^{\bullet} and $\text{GSSG}^{\bullet-}$ radicals. The irradiation conditions are identical to those described in the caption of Figure 1. For reference, the dashed line at $\sim 0.2 \mu\text{s}$ indicates the transition from nonhomogeneous spur kinetics to homogeneous kinetics in the absence of dose rate effects.

Another noteworthy observation is that the $G(-\text{O}_2)$ -vs.-time curve in Figure 3a remains nearly unchanged regardless of the N values used in the simulations. This consistency arises because these N values (20 to 50) are sufficiently low to prevent track overlap before $\sim 3 \times 10^{-8}$ – 10^{-7} s (see Figure 6 of Alanazi et al. [69]). By this time, most R^{\bullet} radicals have already formed via reaction (1) ($\text{RH} + \bullet\text{OH} \rightarrow \text{R}^{\bullet} + \text{H}_2\text{O}$), as the reciprocal of the scavenging power of O_2 at 30 μM towards these radicals ensures that reaction (1) occurs within 2×10^{-9} s. Similarly, the contribution of reaction (R23) remains largely unaffected by dose rate, since most glutathione thiyl radicals are generated through reaction (R17) with $\bullet\text{OH}$ radicals before 10^{-8} s, well before dose rate effects become relevant. Through reaction (R22), these GS^{\bullet} radicals subsequently react with GSH to form $\text{GSSG}^{\bullet-}$, which then reacts with O_2 independently of any dose rate influence.

Using our calculated $G(-\text{O}_2)$ values from Figure 3a, we can then estimate the corresponding concentration of consumed (depleted) oxygen, $[-\text{O}_2]$, over time. This estimation follows the general relationship $C = \rho D G$, where C is concentration, ρ is solution density, D is radiation dose, and G is chemical yield [147]. Assuming a uniform distribution of O_2 molecules within the considered circular cylinder of length 1 μm and radius $R_0 = 0.1 \mu\text{m}$ (see Section 2.1), this concentration, expressed in millimolar, can be directly determined from the following equation [59,148–150]:

$$[-\text{O}_2] \approx 5.3 \times 10^{-4} \times N \times \text{LET} \times G(-\text{O}_2), \quad (8)$$

where $\text{LET} \sim 0.3 \text{ keV}/\mu\text{m}$ for 300-MeV irradiating protons, N is the number of protons per pulse, and $G(-\text{O}_2)$ is in molecules per 100 eV.

Figure 4 illustrates the time evolution of the corresponding consumed oxygen concentrations, calculated using Equation (8) for $N = 20, 30$, and 50 , based on the $G(-\text{O}_2)$ values from our simulations (Figure 3a). As shown, $[-\text{O}_2]$ rises sharply from the microsecond range, reaching an initial, relatively prolonged plateau around 1 millisecond, followed by a second, slightly higher plateau near 1 s. These plateaus increase significantly, roughly proportional to the dose rate.

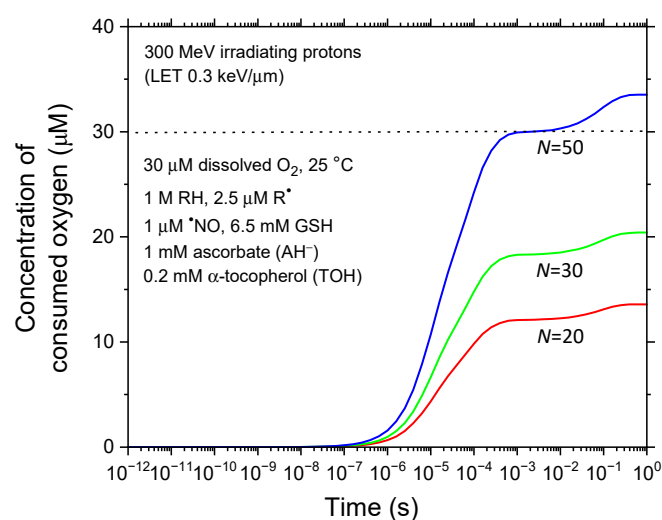


Figure 4. Time dependence of consumed (depleted) oxygen concentration ($[-\text{O}_2]$ in μM) for three values of N , the number of irradiated protons per pulse. The dotted line at $30 \mu\text{M}$ marks the chosen intracellular O_2 concentration. The critical dose rate threshold for effective oxygen depletion and transient hypoxia, optimizing protective effects, is reached at $N \approx 50$.

Notably, our model identifies a critical dose rate threshold below which the FLASH effect, as predicted by the ROD hypothesis, cannot fully manifest. As indicated in Figure 4, this threshold—corresponding to complete oxygen consumption—is reached at $N = 50$. In contrast, at $N = 20$, which represents typical FLASH irradiation conditions with 300 MeV incident protons ($\text{LET} \sim 0.3 \text{ keV}/\mu\text{m}$) delivering $\sim 30 \text{ Gy}$ at an instantaneous dose rate of $\sim 10^6$ – 10^7 Gy/s , only a fraction ($\sim 13.6 \mu\text{M}$ or $\sim 45.3\%$) of the intracellular oxygen ($30 \mu\text{M}$ under our irradiation conditions) is consumed. This comparison with existing experimental data indicates that oxygen depletion alone—and thus the ROD hypothesis—is insufficient to fully explain the observed FLASH effect. These findings align with recent experimental reports challenging the hypothesis that ROD-induced radioresistance alone accounts for the FLASH tissue-sparing effect at clinically relevant doses and dose rates [52–55]. Nonetheless, our model suggests that transient oxygen depletion may play a partial role in the FLASH effect, underscoring the need to explore additional contributing factors.

Figures 5 and 6 examine the sensitivity of our results to two key parameters: the concentration of carbon-based biomolecules (RH), accounting for some cellular heterogeneity, and the diffusion coefficients of reactive species, acknowledging that molecular diffusion in bulk cell water differs significantly from that in pure liquid water. These analyses offer insight into how these factors influence the radiolytic dynamics and the extent of radiolytic oxygen depletion, further refining our understanding of the underlying mechanisms.

In Figure 5, we evaluate the impact of reducing the intracellular bio-organic molecule concentration $[\text{RH}]$ from 1 M to 0.5 M on oxygen consumption under representative FLASH irradiation conditions. Using 300 MeV incident protons ($\text{LET} \sim 0.3 \text{ keV}/\mu\text{m}$) with $N = 20$ and 30 irradiating protons per pulse, we observe that the depleted oxygen concentration

$[-O_2]$ is lower when $[RH]$ is reduced to 0.5 M compared to 1 M. Specifically, for $N = 20$, which corresponds to delivering ~ 30 Gy at an instantaneous dose rate of $\sim 10^6$ – 10^7 Gy/s, $[-O_2]$ decreases from ~ 13.6 μM to 12.3 μM when $[RH]$ is lowered from 1 M to 0.5 M—representing a $\sim 10\%$ decrease. This reduction in oxygen consumption is expected, as a lower $[RH]$ decreases the concentration of R^\bullet radicals through reaction (1) $RH + \bullet OH \rightarrow R^\bullet + H_2O$, thereby reducing the formation of peroxy radicals (ROO^\bullet) via reaction (2) $R^\bullet + O_2 \rightarrow ROO^\bullet$ (see Figure 3b).

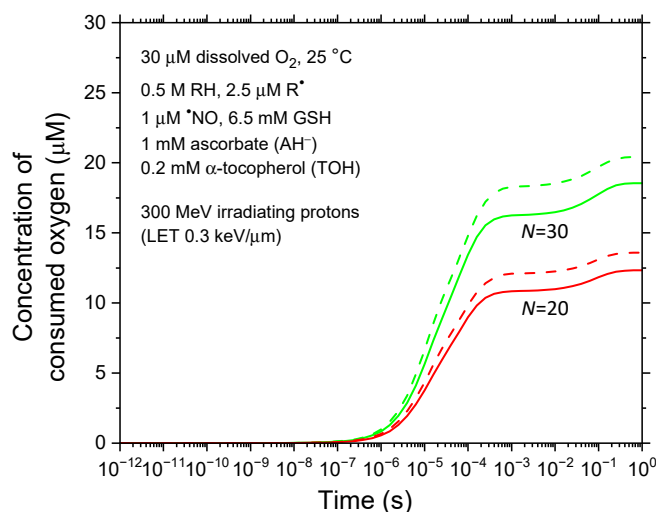


Figure 5. Time evolution of consumed (depleted) oxygen concentration ($[-O_2]$ in μM) for two values of N , the number of irradiated protons per pulse, using $[RH] = 0.5$ M (solid lines). For comparison, $[-O_2]$ values obtained with $[RH] = 1$ M (see Figure 4) are depicted as dashed lines. Both simulation scenarios assume an intracellular O_2 concentration of 30 μM .

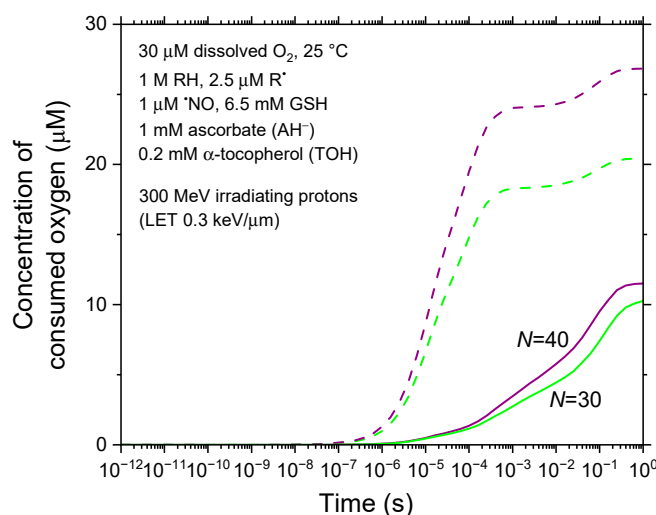


Figure 6. Time evolution of consumed (depleted) oxygen concentration ($[-O_2]$ in μM) for two values of N , the number of irradiated protons per pulse, calculated in a diffusion environment of bulk cell water where all reactive species have diffusion coefficients reduced by a factor of 100 relative to pure liquid water (solid lines). For comparison, $[-O_2]$ values obtained using molecular diffusion in pure liquid water (see Figure 4) are shown as dashed lines. Both simulation scenarios assume an intracellular O_2 concentration of 30 μM .

All simulations presented thus far have assumed that the diffusion coefficients of all reactive species correspond to their values in pure liquid water at room temperature. However, it is well established that intracellular proton (H^+) mobility is approximately

100–300 times slower than in free water [151–153]. To account for the diffusion environment of bulk cell water, we explore a scenario in which the diffusion coefficients of all reactive species are reduced by a factor of 100 relative to their values in pure liquid water. Figure 6 compares the time-dependent consumed O_2 concentrations for $N = 30$ and 40 irradiated protons per pulse under these modified diffusion conditions with those from Figure 4, using identical parameters. Notably, we observe a significant reduction in $[-O_2]$, which decreases from 20.4 μM to 10.3 μM for $N = 30$ at 1 s—representing a more than 50% decrease. This reduction in $[-O_2]$ is even more pronounced for $N = 40$.

These findings, considering both cellular heterogeneity and molecular diffusion in bulk cell water, consistently indicate that the ROD hypothesis alone cannot fully explain the FLASH effect.

4. Conclusions

A leading explanation for the FLASH effect in radiotherapy, the ROD hypothesis, posits that an ultra-short radiation pulse transiently “depletes” intracellular oxygen through radiolytic consumption. This leads to acute hypoxia, temporarily enhancing cellular resistance to radiation. Despite widespread acceptance, the ROD hypothesis continues to be debated. Specifically, the debate primarily focuses on whether the amount of O_2 depleted during pulse irradiation is substantial enough to cause significant hypoxia in well-oxygenated tissues *in vivo*, and whether this can fully account for the observed protective effects of FLASH-RT.

In this study, we employed a computational model to evaluate the ROD hypothesis from a radiation–chemical perspective. We utilized our multi-track chemistry Monte Carlo simulation code, IONLYS-IRT, optimized to model the effects of dose rate on radiolysis within a homogeneous, aerated aqueous environment, mimicking a confined cellular space under instantaneous proton pulses. This medium primarily consisted of water, carbon-based biological molecules (RH), radiation-induced bio-radicals (R^\bullet), glutathione (GSH), ascorbate (AH^-), nitric oxide ($\bullet NO$), and α -tocopherol (TOH). Our model precisely tracked temporal changes in these components, with a special focus on O_2 consumption, from the initial picoseconds up to one second post-exposure.

Among our key findings, the simulations revealed that cellular oxygen is transiently depleted primarily through reactions with R^\bullet radicals and, to a similar extent, with glutathione disulfide radical anions ($GSSG^{\bullet -}$). Contrary to previous reports, we found that the resulting peroxy radicals (ROO^\bullet) are not neutralized via recombination reactions but are instead rapidly scavenged by antioxidants in irradiated cells, notably AH^- and $\bullet NO$. These antioxidants effectively prevent the propagation of damaging peroxidation chain reactions. Thus, our results suggest that antioxidants play a critical role in the FLASH effect, mitigating radiation-induced cellular damage and enhancing radioprotection.

Most importantly, our model identified a critical dose rate threshold below which the FLASH effect, as predicted by the ROD hypothesis, cannot fully manifest. By comparing our results with existing experimental data, we find that the ROD hypothesis alone does not entirely account for the FLASH effect observed in radiotherapy. Our analysis, which also incorporates cellular heterogeneity and molecular diffusion in bulk cell water, consistently suggests that the ROD hypothesis is insufficient to fully explain the FLASH effect. This underscores the complex interplay of cellular responses to high dose-rate radiation and indicates that additional mechanisms or factors, such as alternative oxygen depletion pathways or dynamic cellular responses, are likely involved.

Further research is warranted to identify and quantify these factors that could complement the ROD hypothesis, aiming to provide a more comprehensive understanding of the conditions required to trigger the FLASH effect.

Author Contributions: Conceptualization: I.R., J.-P.J.-G. and J.M.; I.R. conducted the simulations, analyzed and validated the results, and wrote the initial draft of the manuscript based on discussions with J.M. and J.-P.J.-G.; J.M. developed and implemented the model; J.M. and J.-P.J.-G. supervised the work; J.-P.J.-G. reviewed and edited the final version of the manuscript; project administration and funding acquisition was also undertaken by J.-P.J.-G. All authors have read and agreed to the published version of the manuscript.

Funding: This research received funding from the Natural Sciences and Engineering Research Council of Canada (NSERC), under grant number RGPIN-2022-03972, and the Canadian Institutes of Health Research (CIHR), under grant number PJT-195674.

Institutional Review Board Statement: Not applicable.

Informed Consent Statement: Not applicable.

Data Availability Statement: Data generated or analyzed during this study are provided in full within the article.

Acknowledgments: The authors thank J. Richard Wagner and Jean Cadet for fruitful discussions.

Conflicts of Interest: The authors declare no conflicts of interest.

References

- Halperin, E.C.; Brady, L.W.; Perez, C.A.; Wazer, D.E. *Perez & Brady's Principles and Practice of Radiation Oncology*; Lippincott Williams & Wilkins: Philadelphia, PA, USA, 2013.
- Favaudon, V.; Caplier, L.; Monceau, V.; Pouzoulet, F.; Sayarath, M.; Fouillade, C.; Poupon, M.-F.; Brito, I.; Hupé, P.; Bourhis, J.; et al. Ultrahigh dose-rate FLASH irradiation increases the differential response between normal and tumor tissue in mice. *Sci. Transl. Med.* **2014**, *6*, 245ra93. [\[CrossRef\]](#)
- Favaudon, V.; Fouillade, C.; Vozenin, M.-C. Ultrahigh dose-rate, “flash” irradiation minimizes the side-effects of radiotherapy. *Cancer Radiother.* **2015**, *19*, 526–531. [\[CrossRef\]](#) [\[PubMed\]](#)
- Favaudon, V.; Fouillade, C.; Vozenin, M.-C. La radiothérapie FLASH pour épargner les tissus sains. *Med. Sci.* **2015**, *31*, 121–123. [\[CrossRef\]](#)
- Wilson, J.D.; Hammond, E.M.; Higgins, G.S.; Petersson, K. Ultra-high dose rate (FLASH) radiotherapy: Silver bullet or fool’s gold? *Front. Oncol.* **2020**, *9*, 1563. [\[CrossRef\]](#)
- Esplen, N.; Mendonca, M.S.; Bazalova-Carter, M. Physics and biology of ultrahigh dose-rate (FLASH) radiotherapy: A topical review. *Phys. Med. Biol.* **2020**, *65*, 23TR03. [\[CrossRef\]](#) [\[PubMed\]](#)
- Marcu, L.G.; Bezak, E.; Peukert, D.D.; Wilson, P. Translational research in FLASH radiotherapy—From radiobiological mechanisms to in vivo results. *Biomedicine* **2021**, *9*, 181. [\[CrossRef\]](#)
- Gao, Y.; Liu, R.; Chang, C.-W.; Charyyev, S.; Zhou, J.; Bradley, J.D.; Liu, T.; Yang, X. A potential revolution in cancer treatment: A topical review of FLASH radiotherapy. *J. Appl. Clin. Med. Phys.* **2022**, *23*, e13790. [\[CrossRef\]](#)
- Matuszak, N.; Suchorska, W.M.; Milecki, P.; Kruszyna-Mochalska, M.; Misiarz, A.; Pracz, J.; Malicki, J. FLASH radiotherapy: An emerging approach in radiation therapy. *Rep. Pract. Oncol. Radiother.* **2022**, *27*, 344–351. [\[CrossRef\]](#) [\[PubMed\]](#)
- Bogaerts, E.; Macaeva, E.; Isebaert, S.; Haustermans, K. Potential molecular mechanisms behind the ultra-high dose rate “FLASH” effect. *Int. J. Mol. Sci.* **2022**, *23*, 12109. [\[CrossRef\]](#)
- Borghini, A.; Labate, L.; Piccinini, S.; Panaino, C.M.V.; Andreassi, M.G.; Gizzi, L.A. FLASH radiotherapy: Expectations, challenges, and current knowledge. *Int. J. Mol. Sci.* **2024**, *25*, 2546. [\[CrossRef\]](#)
- Tang, R.; Yin, J.; Liu, Y.; Xue, J. FLASH radiotherapy: A new milestone in the field of cancer radiotherapy. *Cancer Lett.* **2024**, *587*, 216651. [\[CrossRef\]](#) [\[PubMed\]](#)
- Bondy, S.C. FLASH radiotherapy versus conventional cancer therapy: Promises, paradoxes and problems. *Int. J. Transl. Med.* **2024**, *4*, 559–569. [\[CrossRef\]](#)
- Chow, J.C.L.; Ruda, H.E. Mechanisms of action in FLASH radiotherapy: A comprehensive review of physicochemical and biological processes on cancerous and normal cells. *Cells* **2024**, *13*, 835. [\[CrossRef\]](#)
- Ma, Y.; Zhang, W.; Zhao, Z.; Lv, J.; Chen, J.; Yan, X.; Lin, X.; Zhang, J.; Wang, B.; Gao, S.; et al. Current views on mechanisms of the FLASH effect in cancer radiotherapy. *Natl. Sci. Rev.* **2024**, *11*, nwae350. [\[CrossRef\]](#)
- Yan, O.; Wang, S.; Wang, Q.; Wang, X. FLASH radiotherapy: Mechanisms of biological effects and the therapeutic potential in cancer. *Biomolecules* **2024**, *14*, 754. [\[CrossRef\]](#) [\[PubMed\]](#)
- Scarmelotto, A.; Delprat, V.; Michiels, C.; Lucas, S.; Heuskin, A.-C. The oxygen puzzle in FLASH radiotherapy: A comprehensive review and experimental outlook. *Clin. Transl. Radiat. Oncol.* **2024**, *49*, 100860. [\[CrossRef\]](#) [\[PubMed\]](#)

18. Shiraishi, Y.; Matsuya, Y.; Fukunaga, H. Possible mechanisms and simulation modeling of FLASH radiotherapy. *Radiol. Phys. Technol.* **2024**, *17*, 11–23. [\[CrossRef\]](#)
19. Li, M.; Zhou, S.; Dong, G.; Wang, C. Emergence of FLASH-radiotherapy across the last 50 years (Review). *Oncol. Lett.* **2024**, *28*, 602. [\[CrossRef\]](#)
20. Wang, Y.; Wang, H.; Hu, J.; Chai, J.; Luan, J.; Li, J.; Xu, Q. FLASH radiotherapy: Mechanisms, nanotherapeutic strategy and future development. *Nanoscale Adv.* **2025**, *7*, 711–721. [\[CrossRef\]](#)
21. Manring, H.R.; Fleming, J.L.; Meng, W.; Gamez, M.E.; Blakaj, D.M.; Chakravarti, A. FLASH radiotherapy: From in vivo data to clinical translation. *Hematol. Oncol. Clin. N. Am.* **2025**, *39*, 237–255. [\[CrossRef\]](#)
22. Friedl, A.A.; Prise, K.M.; Butterworth, K.T.; Montay-Gruel, P.; Favaudon, V. Radiobiology of the FLASH effect. *Med. Phys.* **2022**, *49*, 1993–2013. [\[CrossRef\]](#) [\[PubMed\]](#)
23. Hageman, E.; Che, P.-P.; Dahele, M.; Slotman, B.J.; Sminia, P. Radiobiological aspects of FLASH radiotherapy. *Biomolecules* **2022**, *12*, 1376. [\[CrossRef\]](#) [\[PubMed\]](#)
24. Limoli, C.L.; Vozenin, M.-C. Reinventing radiobiology in the light of FLASH radiotherapy. *Annu. Rev. Cancer Biol.* **2023**, *7*, 1–21. [\[CrossRef\]](#)
25. Rezaee, M.; Iordachita, I.; Wong, J.W. Ultrahigh dose-rate (FLASH) x-ray irradiator for pre-clinical laboratory research. *Phys. Med. Biol.* **2021**, *66*, 095006. [\[CrossRef\]](#)
26. Montay-Gruel, P.; Corde, S.; Laissue, J.A.; Bazalova-Carter, M. FLASH radiotherapy with photon beams. *Med. Phys.* **2022**, *49*, 2055–2067. [\[CrossRef\]](#)
27. Gao, F.; Yang, Y.; Zhu, H.; Wang, J.; Xiao, D.; Zhou, Z.; Dai, T.; Zhang, Y.; Feng, G.; Li, J.; et al. First demonstration of the FLASH effect with ultrahigh dose rate high-energy X-rays. *Radiother. Oncol.* **2022**, *166*, 44–50. [\[CrossRef\]](#)
28. Yang, Y.; Wang, J.; Gao, F.; Liu, Z.; Dai, T.; Zhang, H.; Zhu, H.; Wang, T.; Xiao, D.; Zhou, Z.; et al. FLASH radiotherapy using high-energy X-rays: Current status of PARTER platform in FLASH research. *Radiother. Oncol.* **2024**, *190*, 109967. [\[CrossRef\]](#)
29. Buonanno, M.; Grilj, V.; Brenner, D.J. Biological effects in normal cells exposed to FLASH dose rate protons. *Radiother. Oncol.* **2019**, *139*, 51–55. [\[CrossRef\]](#)
30. Hughes, J.R.; Parsons, J.L. FLASH radiotherapy: Current knowledge and future insights using proton-beam therapy. *Int. J. Mol. Sci.* **2020**, *21*, 6492. [\[CrossRef\]](#)
31. Diffenderfer, E.S.; Sørensen, B.S.; Mazal, A.; Carlson, D.J. The current status of preclinical proton FLASH radiation and future directions. *Med. Phys.* **2022**, *49*, 2039–2054. [\[CrossRef\]](#)
32. Guo, Z.; Buonanno, M.; Harken, A.; Zhou, G.; Hei, T.K. Mitochondrial damage response and fate of normal cells exposed to FLASH irradiation with protons. *Radiat. Res.* **2022**, *197*, 569–582. [\[CrossRef\]](#) [\[PubMed\]](#)
33. Mascia, A.E.; Daugherty, E.C.; Zhang, Y.; Lee, E.; Xiao, Z.; Sertorio, M.; Woo, J.; Backus, L.R.; McDonald, J.M.; McCann, C.; et al. Proton FLASH radiotherapy for the treatment of symptomatic bone metastases: The FAST-01 nonrandomized trial. *JAMA Oncol.* **2023**, *9*, 62–69. [\[CrossRef\]](#)
34. Tessonnier, T.; Mein, S.; Walsh, D.W.M.; Schuhmacher, N.; Liew, H.; Cee, R.; Galonska, M.; Scheloske, S.; Schömers, C.; Weber, U.; et al. FLASH dose rate helium ion beams: First in vitro investigations. *Int. J. Radiat. Oncol. Biol. Phys.* **2021**, *111*, 1011–1022. [\[CrossRef\]](#) [\[PubMed\]](#)
35. Weber, U.; Scifoni, E.; Durante, M. FLASH radiotherapy with carbon ion beams. *Med. Phys.* **2022**, *49*, 1974–1992. [\[CrossRef\]](#) [\[PubMed\]](#)
36. Tinganelli, W.; Weber, U.; Puspitasari, A.; Simoniello, P.; Abdollahi, A.; Oppermann, J.; Schuy, C.; Horst, F.; Helm, A.; Fournier, C.; et al. FLASH with carbon ions: Tumor control, normal tissue sparing, and distal metastasis in a mouse osteosarcoma model. *Radiother. Oncol.* **2022**, *175*, 185–190. [\[CrossRef\]](#)
37. Zakaria, A.M.; Colangelo, N.W.; Meesungnoen, J.; Azzam, E.I.; Plourde, M.-É.; Jay-Gerin, J.-P. Ultra-high dose-rate, pulsed (FLASH) radiotherapy with carbon ions: Generation of early, transient, highly oxygenated conditions in the tumor environment. *Radiat. Res.* **2020**, *194*, 587–593. [\[CrossRef\]](#)
38. Bourhis, J.; Sozzi, W.J.; Jorge, P.G.; Gaide, O.; Bailat, C.; Duclos, F.; Patin, D.; Ozsahin, M.; Bochud, F.; Germond, J.-F.; et al. Treatment of a first patient with FLASH-radiotherapy. *Radiother. Oncol.* **2019**, *139*, 18–22. [\[CrossRef\]](#)
39. Gaide, O.; Herrera, F.; Sozzi, W.J.; Jorge, P.G.; Kinj, R.; Bailat, C.; Duclos, F.; Bochud, F.; Germond, J.-F.; Gondré, M.; et al. Comparison of ultra-high versus conventional dose rate radiotherapy in a patient with cutaneous lymphoma. *Radiother. Oncol.* **2022**, *174*, 87–91. [\[CrossRef\]](#)
40. Spitz, D.R.; Buettner, G.R.; Petronek, M.S.; St-Aubin, J.J.; Flynn, R.T.; Waldron, T.J.; Limoli, C.L. An integrated physico-chemical approach for explaining the differential impact of FLASH versus conventional dose rate irradiation on cancer and normal tissue responses. *Radiother. Oncol.* **2019**, *139*, 23–27. [\[CrossRef\]](#)
41. Pratz, G.; Kapp, D.S. Ultra-high-dose-rate FLASH irradiation may spare hypoxic stem cell niches in normal tissues. *Int. J. Radiat. Oncol. Biol. Phys.* **2019**, *105*, 190–192. [\[CrossRef\]](#)

42. Montay-Gruel, P.; Acharya, M.M.; Petersson, K.; Alikhani, L.; Yakkala, C.; Allen, B.D.; Ollivier, J.; Petit, B.; Gonçalves Jorge, P.; Syage, A.R.; et al. Long-term neurocognitive benefits of FLASH radiotherapy driven by reduced reactive oxygen species. *Proc. Natl. Acad. Sci. USA* **2019**, *116*, 10943–10951. [\[CrossRef\]](#)
43. Pratz, G.; Kapp, D.S. A computational model of radiolytic oxygen depletion during FLASH irradiation and its effect on the oxygen enhancement ratio. *Phys. Med. Biol.* **2019**, *64*, 185005. [\[CrossRef\]](#)
44. Adrian, G.; Konradsson, E.; Lempart, M.; Bäck, S.; Ceberg, C.; Petersson, K. The FLASH effect depends on oxygen concentration. *Br. J. Radiol.* **2020**, *93*, 20190702. [\[CrossRef\]](#)
45. Petersson, K.; Adrian, G.; Butterworth, K.; McMahon, S.J. A quantitative analysis of the role of oxygen tension in FLASH radiation therapy. *Int. J. Radiat. Oncol. Biol. Phys.* **2020**, *107*, 539–547. [\[CrossRef\]](#) [\[PubMed\]](#)
46. Rothwell, B.C.; Kirkby, N.F.; Merchant, M.J.; Chadwick, A.L.; Lowe, M.; Mackay, R.I.; Hendry, J.H.; Kirkby, K.J. Determining the parameter space for effective oxygen depletion for FLASH radiation therapy. *Phys. Med. Biol.* **2021**, *66*, 055020. [\[CrossRef\]](#)
47. Favaudon, V.; Labarbe, R.; Limoli, C.L. Model studies of the role of oxygen in the FLASH effect. *Med. Phys.* **2022**, *49*, 2068–2081. [\[CrossRef\]](#) [\[PubMed\]](#)
48. Dewey, D.L.; Boag, J.W. Modification of the oxygen effect when bacteria are given large pulses of radiation. *Nature* **1959**, *183*, 1450–1451. [\[CrossRef\]](#)
49. Weiss, H.; Epp, E.R.; Heslin, J.M.; Ling, C.C.; Santomasso, A. Oxygen depletion in cells irradiated at ultra-high dose-rates and at conventional dose-rates. *Int. J. Radiat. Biol.* **1974**, *26*, 17–29. [\[CrossRef\]](#)
50. Epp, E.R.; Weiss, H.; Ling, C.C. Irradiation of cells by single and double pulses of high intensity radiation: Oxygen sensitization and diffusion kinetics. *Curr. Top. Radiat. Res. Q* **1976**, *11*, 201–250, Corpus ID: 21836789.
51. Wilson, P.; Jones, B.; Yokoi, T.; Hill, M.; Vojnovic, B. Revisiting the ultra-high dose rate effect: Implications for charged particle radiotherapy using protons and light ions. *Br. J. Radiol.* **2012**, *85*, e933–e939. [\[CrossRef\]](#)
52. Cao, X.; Zhang, R.; Esipova, T.V.; Allu, S.R.; Ashraf, R.; Rahman, M.; Gunn, J.R.; Bruza, P.; Gladstone, D.J.; Williams, B.B.; et al. Quantification of oxygen depletion during FLASH irradiation in vitro and in vivo. *Int. J. Radiat. Oncol. Biol. Phys.* **2021**, *111*, 240–248. [\[CrossRef\]](#) [\[PubMed\]](#)
53. Jansen, J.; Knoll, J.; Beyreuther, E.; Pawelke, J.; Skuza, R.; Hanley, R.; Brons, S.; Pagliari, F.; Seco, J. Does FLASH deplete oxygen? Experimental evaluation for photons, protons, and carbon ions. *Med. Phys.* **2021**, *48*, 3982–3990. [\[CrossRef\]](#)
54. El Khatib, M.; van Slyke, A.L.; Velalopoulou, A.; Kim, M.M.; Shoniyozov, K.; Allu, S.R.; Diffenderfer, E.S.; Busch, T.M.; Wiersma, R.D.; Koch, C.J.; et al. Ultrafast tracking of oxygen dynamics during proton FLASH. *Int. J. Radiat. Oncol. Biol. Phys.* **2022**, *113*, 624–634. [\[CrossRef\]](#) [\[PubMed\]](#)
55. Grilj, V.; Leavitt, R.J.; El Khatib, M.; Paisley, R.; Franco-Perez, J.; Petit, B.; Ballesteros-Zebadua, P.; Vozenin, M.-C. In vivo measurements of change in tissue oxygen level during irradiation reveal novel dose rate dependence. *Radiother. Oncol.* **2024**, *201*, 110539. [\[CrossRef\]](#) [\[PubMed\]](#)
56. Bensasson, R.V.; Land, E.J.; Truscott, T.G. *Excited States and Free Radicals in Biology and Medicine. Contributions from Flash Photolysis and Pulse Radiolysis*; Oxford University Press: Oxford, UK, 1993.
57. Spinks, J.W.T.; Woods, R.J. *An Introduction to Radiation Chemistry*; Wiley: New York, NY, USA, 1990.
58. LaVerne, J.A. Radiation chemical effects of heavy ions. In *Charged Particle and Photon Interactions with Matter: Chemical, Physicochemical, and Biological Consequences with Applications*; Mozumder, A., Hatano, Y., Eds.; Marcel Dekker: New York, NY, USA, 2004; pp. 403–429.
59. Meesungnoen, J.; Jay-Gerin, J.-P. Radiation chemistry of liquid water with heavy ions: Monte Carlo simulations studies. In *Charged Particle and Photon Interactions with Matter: Recent Advances, Applications, and Interfaces*; Hatano, Y., Katsumura, Y., Mozumder, A., Eds.; Taylor & Francis: Boca Raton, FL, USA, 2011; pp. 355–400.
60. Bielski, B.H.J.; Cabelli, D.E.; Arudi, R.L.; Ross, A.B. Reactivity of HO_2/O_2^- radicals in aqueous solution. *J. Phys. Chem. Ref. Data* **1985**, *14*, 1041–1100. [\[CrossRef\]](#)
61. Michaels, H.B.; Hunt, J.W. A model for radiation damage in cells by direct effect and by indirect effect: A radiation chemistry approach. *Radiat. Res.* **1978**, *74*, 23–34. [\[CrossRef\]](#)
62. Labarbe, R.; Hotoiu, L.; Barbier, J.; Favaudon, V. A physicochemical model of reaction kinetics supports peroxy radical recombination as the main determinant of the FLASH effect. *Radiother. Oncol.* **2020**, *153*, 303–310. [\[CrossRef\]](#)
63. Wardman, P. Approaches to modeling chemical reaction pathways in radiobiology. *Int. J. Radiat. Biol.* **2022**, *98*, 1399–1413. [\[CrossRef\]](#)
64. Wardman, P. Radiotherapy using high-intensity pulsed radiation beams (FLASH): A radiation-chemical perspective. *Radiat. Res.* **2020**, *194*, 607–617. [\[CrossRef\]](#)
65. Hu, A.; Qiu, R.; Li, W.B.; Zhou, W.; Wu, Z.; Zhang, H.; Li, J. Radical recombination and antioxidants: A hypothesis on the FLASH effect mechanism. *Int. J. Radiat. Biol.* **2023**, *99*, 620–628. [\[CrossRef\]](#)
66. Hu, A.; Zhou, W.; Qiu, R.; Wei, S.; Wu, Z.; Zhang, H.; Li, J. Computational model of radiation oxygen effect with Monte Carlo simulation: Effects of antioxidants and peroxy radicals. *Int. J. Radiat. Biol.* **2024**, *100*, 595–608. [\[CrossRef\]](#) [\[PubMed\]](#)

67. Tan, H.S.; Teo, K.B.K.; Dong, L.; Friberg, A.; Koumenis, C.; Diffenderfer, E.; Zou, J.W. Modeling ultra-high dose rate electron and proton FLASH effect with the physicochemical approach. *Phys. Med. Biol.* **2023**, *68*, 145013. [\[CrossRef\]](#)
68. Sultana, A.; Alanazi, A.; Meesungnoen, J.; Jay-Gerin, J.-P. On the transient radiolytic oxygen depletion in the ultra-high (FLASH) dose-rate radiolysis of water in a cell-like environment: Effect of e^-_{aq} and $\bullet OH$ competing scavengers. *Radiat. Res.* **2022**, *197*, 566–567. [\[CrossRef\]](#)
69. Alanazi, A.; Meesungnoen, J.; Jay-Gerin, J.-P. A computer modeling study of water radiolysis at high dose rates. Relevance to FLASH radiotherapy. *Radiat. Res.* **2021**, *195*, 149–162. [\[CrossRef\]](#)
70. Lai, Y.; Jia, X.; Chi, Y. Modeling the effect of oxygen on the chemical stage of water radiolysis using GPU-based microscopic Monte Carlo simulations, with an application in FLASH radiotherapy. *Phys. Med. Biol.* **2021**, *66*, 025004. [\[CrossRef\]](#)
71. Zhu, H.; Li, J.; Deng, X.; Qiu, R.; Wu, Z.; Zhang, H. Modeling of cellular response after FLASH irradiation: A quantitative analysis based on the radiolytic oxygen depletion hypothesis. *Phys. Med. Biol.* **2021**, *66*, 185009. [\[CrossRef\]](#)
72. Boscolo, D.; Scifoni, E.; Durante, M.; Krämer, M.; Fuss, M.C. May oxygen depletion explain the FLASH effect? A chemical track structure analysis. *Radiother. Oncol.* **2021**, *162*, 68–75. [\[CrossRef\]](#)
73. Farokhi, F.; Shirani, B.; Fattori, S.; Asgarian, M.A.; Cuttone, G.; Jia, S.B.; Petringa, G.; Sciuto, A.; Cirrone, G.A.P. Effects of the oxygen depletion in FLASH irradiation investigated through Geant4-DNA toolkit. *Radiat. Phys. Chem.* **2023**, *212*, 111184. [\[CrossRef\]](#)
74. Buxton, G.V.; Greenstock, C.L.; Helman, W.P.; Ross, A.B. Critical review of rate constants for reactions of hydrated electrons, hydrogen atoms and hydroxyl radicals ($\bullet OH/\bullet O^-$) in aqueous solution. *J. Phys. Chem. Ref. Data* **1988**, *17*, 513–886. [\[CrossRef\]](#)
75. von Sonntag, C. *Free-Radical-Induced DNA Damage and Its Repair: A Chemical Perspective*; Springer: Berlin/Heidelberg, Germany, 2006; pp. 159–194.
76. Alfassi, Z.B.; Huie, R.E.; Neta, P. Kinetic studies of organic peroxy radicals in aqueous solutions and mixed solvents. In *Peroxy Radicals*; Alfassi, Z.B., Ed.; Wiley: Chichester, UK, 1997; pp. 235–281.
77. Neta, P.; Huie, R.E.; Ross, A.B. Rate constants for reactions of peroxy radicals in fluid solutions. *J. Phys. Chem. Ref. Data* **1990**, *19*, 413–513. [\[CrossRef\]](#)
78. Ingold, K.U. Peroxy radicals. *Acc. Chem. Res.* **1969**, *2*, 1–9. [\[CrossRef\]](#)
79. Alfassi, Z.B. (Ed.) *Peroxy Radicals*; Wiley: Chichester, UK, 1997.
80. Yin, H.; Xu, L.; Porter, N.A. Free radical lipid peroxidation: Mechanisms and analysis. *Chem. Rev.* **2011**, *111*, 5944–5972. [\[CrossRef\]](#) [\[PubMed\]](#)
81. Azzam, E.I.; Jay-Gerin, J.-P.; Pain, D. Ionizing radiation-induced metabolic oxidative stress and prolonged cell injury. *Cancer Lett.* **2012**, *327*, 48–60. [\[CrossRef\]](#) [\[PubMed\]](#)
82. Halliwell, B.; Gutteridge, J.M.C. *Free Radicals in Biology and Medicine*; Oxford University Press: Oxford, UK, 2015.
83. Robert, G.; Wagner, J.R.; Cadet, J. Oxidatively generated tandem DNA modifications by pyrimidinyl and 2-deoxyribosyl peroxy radicals. *Free Radic. Biol. Med.* **2023**, *196*, 22–36. [\[CrossRef\]](#)
84. Hall, E.J.; Giaccia, A.J. *Radiobiology for the Radiologist*, 8th ed.; Wolters Kluwer: Philadelphia, PA, USA, 2019.
85. Baatout, S. (Ed.) *Radiobiology Textbook*; Belgian Nuclear Research Centre (SCK CEN): Mol, Belgium; Springer: Cham, Switzerland, 2023. [\[CrossRef\]](#)
86. Kuppermann, A. Diffusion kinetics in radiation chemistry. In *Actions Chimiques et Biologiques des Radiations*; Haïssinsky, M., Ed.; Masson: Paris, France, 1961; Volume 5, pp. 85–166.
87. Bepari, M.I.; Meesungnoen, J.; Jay-Gerin, J.-P. Early and transient formation of highly acidic pH spikes in water radiolysis under the combined effect of high dose rate and high linear energy transfer. *Radiation* **2023**, *3*, 165–182. [\[CrossRef\]](#)
88. Baikalov, A.; Abolfath, R.; Schüller, E.; Mohan, R.; Wilkens, J.J.; Bartzsch, S. Intertrack interaction at ultra-high dose rates and its role in the FLASH effect. *Front. Phys.* **2023**, *11*, 1215422. [\[CrossRef\]](#)
89. Furchgott, R.S.; Zawadki, J.V. The obligatory role of endothelial cells in the relaxation of arterial smooth muscle by acetylcholine. *Nature* **1980**, *288*, 373–376. [\[CrossRef\]](#)
90. Moncada, S.; Palmer, R.M.J.; Higgs, E.A. Nitric oxide: Physiology, pathophysiology, and pharmacology. *Pharmacol. Rev.* **1991**, *43*, 109–142.
91. Fukuto, J.M.; Wink, D.A. Nitric oxide (NO): Formation and biological roles in mammalian systems. In *Metal Ions in Biological Systems*; Sigel, A., Sigel, H., Eds.; Marcel Dekker: New York, NY, USA, 1999; Volume 36, pp. 547–595.
92. Jay-Gerin, J.-P.; Ferradini, C. Are there protective enzymatic pathways to regulate high local nitric oxide ($\bullet NO$) concentrations in cells under stress conditions? *Biochimie* **2000**, *82*, 161–166. [\[CrossRef\]](#)
93. Toledo, J.C., Jr.; Augusto, O. Connecting the chemical and biological properties of nitric oxide. *Chem. Res. Toxicol.* **2012**, *25*, 975–989. [\[CrossRef\]](#)
94. Belenichev, I.; Popazova, O.; Bukhtiyarova, N.; Savchenko, D.; Oksenysh, V.; Kamysnyy, O. Modulating nitric oxide: Implications for cytotoxicity and cytoprotection. *Antioxidants* **2024**, *13*, 504. [\[CrossRef\]](#) [\[PubMed\]](#)
95. Beckman, J.S. Ischaemic injury mediator. *Nature* **1990**, *345*, 27–28. [\[CrossRef\]](#) [\[PubMed\]](#)

96. Goldstein, S.; Czapski, G. The reaction of NO^\bullet with $\text{O}_2^{\bullet-}$ and HO_2^\bullet : A pulse radiolysis study. *Free Radic. Biol. Med.* **1995**, *19*, 505–510. [[CrossRef](#)]
97. Kissner, R.; Nauser, T.; Bugnon, P.; Lye, P.G.; Koppenol, W.H. Formation and properties of peroxynitrite as studied by laser flash photolysis, high-pressure stopped-flow technique, and pulse radiolysis. *Chem. Res. Toxicol.* **1997**, *10*, 1285–1292. [[CrossRef](#)] [[PubMed](#)]
98. Padmaja, S.; Huie, R.E. The reaction of nitric oxide with organic peroxy radicals. *Biochem. Biophys. Res. Commun.* **1993**, *195*, 539–544. [[CrossRef](#)]
99. Hogg, N.; Kalyanaraman, B. Nitric oxide and lipid peroxidation. *Biochim. Biophys. Acta* **1999**, *1411*, 378–384. [[CrossRef](#)]
100. Korytowski, W.; Zareba, M.; Girotti, A.W. Inhibition of free radical-mediated cholesterol peroxidation by diazeniumdiolate-derived nitric oxide: Effect of release rate on mechanism of action in a membrane system. *Chem. Res. Toxicol.* **2000**, *13*, 1265–1274. [[CrossRef](#)]
101. Darley-Usmar, V.M.; Patel, R.P.; O'Donnell, V.B.; Freeman, B.A. Antioxidant actions of nitric oxide. In *Nitric Oxide. Biology and Pathobiology*; Ignarro, L.J., Ed.; Academic Press: San Diego, CA, USA, 2000; Chapter 17; pp. 265–276.
102. Rubbo, H.; Radi, R.; Anselmi, D.; Kirk, M.; Barnes, S.; Butler, J.; Eiserich, J.P.; Freeman, B.A. Nitric oxide reaction with lipid peroxy radical spares α -tocopherol during lipid peroxidation. *J. Biol. Chem.* **2000**, *275*, 10812–10818. [[CrossRef](#)]
103. Boveris, A.; Poderoso, J.J. Regulation of oxygen metabolism by nitric oxide. In *Nitric Oxide: Biology and Pathobiology*; Ignarro, L.J., Ed.; Academic Press: San Diego, CA, USA, 2000; Chapter 23; pp. 355–368.
104. Hall, C.N.; Garthwaite, J. What is the real physiological NO concentration in vivo? *Nitric Oxide* **2009**, *21*, 92–103. [[CrossRef](#)]
105. Kennedy, L.; Sandhu, J.K.; Harper, M.-E.; Cuperlovic-Culf, M. Role of glutathione in cancer: From mechanisms to therapies. *Biomolecules* **2020**, *10*, 1429. [[CrossRef](#)]
106. Babbs, C.F.; Steiner, M.G. Simulation of free radical reactions in biology and medicine: A new two-compartment kinetic model of intracellular lipid peroxidation. *Free Radic. Biol. Med.* **1990**, *8*, 471–485. [[CrossRef](#)] [[PubMed](#)]
107. Wahlländer, A.; Soboll, S.; Sies, H.; Linke, I.; Müller, M. Hepatic mitochondrial and cytosolic glutathione content and the subcellular distribution of GHS-S-transferases. *FEBS Lett.* **1979**, *97*, 138–140. [[CrossRef](#)] [[PubMed](#)]
108. Arteel, G.E.; Briviba, K.; Sies, H. Mechanisms of antioxidant defense against nitric oxide/peroxynitrite. In *Nitric Oxide: Biology and Pathobiology*; Ignarro, L.J., Ed.; Academic Press: San Diego, CA, USA, 2000; Chapter 22; pp. 343–354.
109. Robert, G.; Wagner, J.R. Scavenging of alkylperoxy radicals by addition to ascorbate: An alternative mechanism to electron transfer. *Antioxidants* **2024**, *13*, 1194. [[CrossRef](#)]
110. Jackson, T.S.; Xu, A.; Vita, J.A.; Keaney, J.F., Jr. Ascorbate prevents the interaction of superoxide and nitric oxide only at very high physiological concentrations. *Circ. Res.* **1998**, *83*, 916–922. [[CrossRef](#)]
111. Shen, J.; Griffiths, P.T.; Campbell, S.J.; Uttinger, B.; Kalberer, M.; Paulson, S.E. Ascorbate oxidation by iron, copper and reactive oxygen species: Review, model development, and derivation of key rate constants. *Sci. Rep.* **2021**, *11*, 7417. [[CrossRef](#)]
112. Tu, Y.-J.; Njus, D.; Schlegel, H.B. A theoretical study of ascorbic acid oxidation and $\text{HOO}^\bullet/\text{O}_2^{\bullet-}$ radical scavenging. *Org. Biomol. Chem.* **2017**, *15*, 4417–4431. [[CrossRef](#)]
113. Bielski, B.H.J. Chemistry of ascorbic acid radicals. In *Ascorbic Acid: Chemistry, Metabolism, and Uses*; Seib, P., Tolbert, B.M., Eds.; American Chemical Society: Washington, DC, USA, 1982; Chapter 4; pp. 81–100. [[CrossRef](#)]
114. Njus, D.; Kelley, P.M.; Tu, Y.-J.; Schlegel, H.B. Ascorbic acid: The chemistry underlying its antioxidant properties. *Free. Radic. Biol. Med.* **2020**, *159*, 37–43. [[CrossRef](#)]
115. Buettner, G.R.; Jurkiewicz, B.A. Catalytic metals, ascorbate and free radicals: Combinations to avoid. *Radiat. Res.* **1996**, *145*, 532–541. [[CrossRef](#)]
116. Wardman, P. Some applications of radiation chemistry to biochemistry and radiobiology. In *Radiation Chemistry: Principles and Applications*; Farhataziz, Rodgers, M.A.J., Eds.; VCH Publishers: New York, NY, USA, 1987; pp. 565–599.
117. Priyadarsini, K.I. Redox reactions of antioxidants: Contributions from radiation chemistry of aqueous solutions. In *Charged Particle and Photon Interactions with Matter: Recent Advances, Applications, and Interfaces*; Hatano, Y., Katsumura, Y., Mozumder, A., Eds.; Taylor & Francis: Boca Raton, FL, USA, 2011; pp. 595–622.
118. Packer, J.E.; Slater, T.F.; Willson, R.L. Direct observation of a free radical interaction between vitamin E and vitamin C. *Nature* **1979**, *278*, 737–738. [[CrossRef](#)]
119. Forni, L.G. Free radical reactions involving fatty acids: The pulse radiolysis approach. In *Membrane Lipid Oxidation*; Vigo-Pelfrey, C., Ed.; CRC Press: Boca Raton, FL, USA, 1990; Volume 1, pp. 15–32.
120. Penabei, S.; Meesungnoen, J.; Jay-Gerin, J.-P. Assessment of cystamine's radioprotective/antioxidant ability under high-dose-rate irradiation: A Monte Carlo multi-track chemistry simulation study. *Antioxidants* **2023**, *12*, 776. [[CrossRef](#)]
121. Mustaree, S.; Meesungnoen, J.; Butarbutar, S.L.; Causey, P.; Stuart, C.R.; Jay-Gerin, J.-P. Self-radiolysis of tritiated water. 3. The $^\bullet\text{OH}$ scavenging effect of bromide ions on the yield of H_2O_2 in the radiolysis of water by ^{60}Co γ -rays and tritium β -particles at room temperature. *RSC Adv.* **2014**, *4*, 43572–43581. [[CrossRef](#)]

122. *The Dosimetry of Pulsed Radiation*; ICRU Report No. 34; International Commission on Radiation Units and Measurements: Bethesda, MD, USA, 1982.
123. Cobut, V.; Frongillo, Y.; Patau, J.P.; Goulet, T.; Fraser, M.-J.; Jay-Gerin, J.-P. Monte Carlo simulation of fast electron and proton tracks in liquid water—I. Physical and physicochemical aspects. *Radiat. Phys. Chem.* **1998**, *51*, 229–243. [\[CrossRef\]](#)
124. Frongillo, Y.; Goulet, T.; Fraser, M.-J.; Cobut, V.; Patau, J.P.; Jay-Gerin, J.-P. Monte Carlo simulation of fast electron and proton tracks in liquid water—II. Nonhomogeneous chemistry. *Radiat. Phys. Chem.* **1998**, *51*, 245–254. [\[CrossRef\]](#)
125. Tachiya, M. Theory of diffusion-controlled reactions: Formulation of the bulk reaction rate in terms of the pair probability. *Radiat. Phys. Chem.* **1983**, *21*, 167–175. [\[CrossRef\]](#)
126. Pimblott, S.M.; Pilling, M.J.; Green, N.J.B. Stochastic models of spur kinetics in water. *Radiat. Phys. Chem.* **1991**, *37*, 377–388. [\[CrossRef\]](#)
127. Pimblott, S.M.; Green, N.J.B. Recent advances in the kinetics of radiolytic processes. In *Research in Chemical Kinetics*; Compton, R.G., Hancock, G., Eds.; Elsevier: Amsterdam, The Netherlands, 1995; Volume 3, pp. 117–174. [\[CrossRef\]](#)
128. Goulet, T.; Fraser, M.-J.; Frongillo, Y.; Jay-Gerin, J.-P. On the validity of the independent reaction times approximation for the description of the nonhomogeneous kinetics of liquid water radiolysis. *Radiat. Phys. Chem.* **1998**, *51*, 85–91. [\[CrossRef\]](#)
129. Wardman, P. Radiation-chemical perspective of the radiobiology of pulsed (high dose-rate) radiation (FLASH): A postscript. *Radiat. Res.* **2024**, *201*, 87–91. [\[CrossRef\]](#)
130. Qian, S.Y.; Buettner, G.R. Iron and dioxygen chemistry is an important route to initiation of biological free radical oxidations: An electron paramagnetic resonance spin trapping study. *Free Radic. Biol. Med.* **1999**, *26*, 1447–1456. [\[CrossRef\]](#) [\[PubMed\]](#)
131. von Sonntag, C. The chemistry of free-radical-mediated DNA damage. In *Physical and Chemical Mechanisms in Molecular Radiation Biology*; Glass, W.A., Varma, M.N., Eds.; Plenum Press: New York, NY, USA, 1991; pp. 287–321.
132. Mee, L.K. Radiation chemistry of biopolymers. In *Radiation Chemistry: Principles and Applications*; Farhataziz, Rodgers, M.A.J., Eds.; VCH Publishers: New York, NY, USA, 1987; pp. 477–499.
133. Anbar, M.; Farhataziz; Ross, A.B. *Selected Specific Rates of Reactions of Transients from Water in Aqueous Solution. II. Hydrogen Atom*; Report No. NERDS-NBS 51; US Government Printing Office: Washington, DC, USA, 1975.
134. Fielden, E.M.; Roberts, P.B.; Bray, R.C.; Lowe, D.J.; Mautner, G.N.; Rotilio, G.; Calabrese, L. The mechanism of action of superoxide dismutase from pulse radiolysis and electron paramagnetic resonance. Evidence that only half the active sites function in catalysis. *Biochem. J.* **1974**, *139*, 49–60. [\[CrossRef\]](#)
135. Bothe, E.; Schuchmann, M.N.; Schulte-Frohlinde, D.; von Sonntag, C. Hydroxyl radical-induced oxidation of ethanol in oxygenated aqueous solutions. A pulse radiolysis and product study. *Z. Naturforsch. B* **1983**, *38*, 212–219. [\[CrossRef\]](#)
136. Meesat, R.; Sanguanmith, S.; Meesungnoen, J.; Lepage, M.; Khalil, A.; Jay-Gerin, J.-P. Utilization of the ferrous sulfate (Fricke) dosimeter for evaluating the radioprotective potential of cystamine: Experiment and Monte Carlo simulation. *Radiat. Res.* **2012**, *177*, 813–826. [\[CrossRef\]](#) [\[PubMed\]](#)
137. Abedinzadeh, Z.; Gardès-Albert, M.; Ferradini, C. Reactions of $\bullet\text{OH}$ and $\text{Br}_2^{\bullet-}$ radicals with glutathione. A radiolysis study. *Radiat. Phys. Chem.* **1992**, *40*, 551–558. [\[CrossRef\]](#)
138. Mezyk, S.P. Rate constant determination for the reaction of hydroxyl and glutathione thiyl radicals with glutathione in aqueous solution. *J. Phys. Chem.* **1996**, *100*, 8861–8866. [\[CrossRef\]](#)
139. Wardman, P. Thiyl radicals in biology: Their role as a ‘molecular switch’ central to cellular oxidative stress. In *S-Centered Radicals*; Alfassi, Z.B., Ed.; Wiley: Chichester, UK, 1999; pp. 289–309.
140. Wardman, P.; von Sonntag, C. Kinetic factors that control the fate of thiyl radicals in cells. *Methods Enzymol.* **1995**, *251*, 31–45. [\[CrossRef\]](#)
141. Nauser, T.; Koppenol, W.H.; Schöneich, C. Protein thiyl radical reactions and product formation: A kinetic simulation. *Free Radic. Biol. Med.* **2015**, *80*, 158–163. [\[CrossRef\]](#)
142. Madej, E.; Folkes, L.K.; Wardman, P.; Czapski, G.; Goldstein, S. Thiyl radicals react with nitric oxide to form S-nitrosothiols with rate constants near the diffusion-controlled limit. *Free Radic. Biol. Med.* **2008**, *44*, 2013–2018. [\[CrossRef\]](#)
143. Huie, R.E.; Padmaja, S. The reaction of NO with superoxide. *Free Radic. Res. Commun.* **1993**, *18*, 195–199. [\[CrossRef\]](#) [\[PubMed\]](#)
144. Bartlett, D.; Church, D.F.; Bounds, P.L.; Koppenol, W.H. The kinetics of the oxidation of L-ascorbic acid by peroxyxynitrite. *Free Radic. Biol. Med.* **1995**, *18*, 85–92. [\[CrossRef\]](#)
145. Keszler, A.; Zhang, Y.; Hogg, N. Reaction between nitric oxide, glutathione, and oxygen in the presence and absence of protein: How are S-nitrosothiols formed? *Free Radic. Biol. Med.* **2010**, *48*, 55–64. [\[CrossRef\]](#)
146. Sanguanmith, S.; Meesungnoen, J.; Muroya, Y.; Lin, M.; Katsumura, Y.; Jay-Gerin, J.-P. On the spur lifetime and its temperature dependence in the low linear energy transfer radiolysis of water. *Phys. Chem. Chem. Phys.* **2012**, *14*, 16731–16736. [\[CrossRef\]](#)
147. Hummel, A. *Radiation Chemistry: The Chemical Effects of Ionizing Radiation and Their Applications*; Interfaculty Reactor Institute-Technische Universiteit Delft (IRI-DUT): Delft, The Netherlands, 1995.
148. Schardt, D.; Elsässer, T.; Schulz-Ertner, D. Heavy-ion tumor therapy: Physical and radiobiological benefits. *Rev. Mod. Phys.* **2010**, *82*, 383–425. [\[CrossRef\]](#)

149. Baverstock, K.F.; Burns, W.G. Primary production of oxygen from irradiated water as an explanation for decreased radiobiological oxygen enhancement at high LET. *Nature* **1976**, *260*, 316–318. [[CrossRef](#)] [[PubMed](#)]
150. Pimblott, S.M.; LaVerne, J.A. Effects of track structure on the ion radiolysis of the Fricke dosimeter. *J. Phys. Chem. A* **2002**, *106*, 9420–9427. [[CrossRef](#)]
151. Negendank, W.; Edelman, L. *The State of Water in the Cell*; Scanning Microscopy International: Chicago, IL, USA, 1988.
152. Swietach, P.; Vaughan-Jones, R.D. Relationship between intracellular pH and proton mobility in rat and guinea-pig ventricular myocytes. *J. Physiol.* **2005**, *566*, 793–806. [[CrossRef](#)]
153. Islam, M.M.; Kanike, V.; Meesungnoen, J.; Lertnaisat, P.; Katsumura, Y.; Jay-Gerin, J.-P. In situ generation of ultrafast transient “acid spikes” in the $^{10}\text{B}(n,\alpha)^7\text{Li}$ radiolysis of water. *Chem. Phys. Lett.* **2018**, *693*, 210–215. [[CrossRef](#)]

Disclaimer/Publisher’s Note: The statements, opinions and data contained in all publications are solely those of the individual author(s) and contributor(s) and not of MDPI and/or the editor(s). MDPI and/or the editor(s) disclaim responsibility for any injury to people or property resulting from any ideas, methods, instructions or products referred to in the content.